GENERATION AND ANALYSIS OF "BREATHING" AS AN HRI BEHAVIOR ON A COBOT

A THESIS SUBMITTED TO
THE GRADUATE SCHOOL OF NATURAL AND APPLIED SCIENCES
OF
MIDDLE EAST TECHNICAL UNIVERSITY

BY

ALİ NURİ GÜNEŞDOĞDU

IN PARTIAL FULFILLMENT OF THE REQUIREMENTS
FOR
THE DEGREE OF MASTER OF SCIENCE
IN
COMPUTER ENGINEERING

AUGUST 2022

Approval of the thesis:

GENERATION AND ANALYSIS OF "BREATHING" AS AN HRI BEHAVIOR ON A COBOT

submitted by **ALİ NURİ GÜNEŞDOĞDU** in partial fulfillment of the requirements for the degree of **Master of Science in Computer Engineering Department, Middle East Technical University** by,

Prof. Dr. Halil Kalıpçılar
Dean, Graduate School of **Natural and Applied Sciences** _____

Prof. Dr. Halit Oğuztüzün
Head of Department, **Computer Engineering** _____

Assoc. Prof. Dr. Erol Şahin
Supervisor, **Computer Engineering, METU** _____

Assoc. Prof. Dr. Cengiz Acartürk
Co-supervisor, **Graduate School of Informatics, METU** _____

Examining Committee Members:

Assoc. Prof. Dr. Sinan Kalkan
Computer Engineering, METU _____

Assoc. Prof. Dr. Erol Şahin
Computer Engineering, METU _____

Assist. Prof. Dr. Barış Akgün
Computer Engineering, Koç University _____

Date:31.08.2022

I hereby declare that all information in this document has been obtained and presented in accordance with academic rules and ethical conduct. I also declare that, as required by these rules and conduct, I have fully cited and referenced all material and results that are not original to this work.

Name, Surname: Ali Nuri Güneşdoğdu

Signature :

ABSTRACT

GENERATION AND ANALYSIS OF "BREATHING" AS AN HRI BEHAVIOR ON A COBOT

Güneşdoğdu, Ali Nuri
M.S., Department of Computer Engineering
Supervisor: Assoc. Prof. Dr. Erol Şahin
Co-Supervisor: Assoc. Prof. Dr. Cengiz Acartürk

August 2022, 69 pages

Collaborative robots, a.k.a cobots, are industrial robotic manipulators that have no built-in capabilities for social human-robot interaction (HRI). In the thesis, we implemented *breathing* for a cobot as a social behavior inspired by the *secondary action* animation principle. We automatically generated *breathing* of a cobot as HRI behavior with its waveform borrowed from human breathing; its amplitude and frequency are parametrized.

We conducted a user study to measure the effect of parameters of *breathing* behavior on a collaborative task. During the study, we collected the task completion time to evaluate the task performance and velocities and accelerations of the hand of subjects to evaluate the task quality. We measured HRI quality using the Godspeed questionnaire. The analysis showed that a frequency similar to a human's breathing positively impacts task performance and improves task quality; however, it did not significantly affect HRI quality. Besides, changing the amplitude of the breathing did not affect any metrics.

Keywords: Collaborative robot, human-robot interaction, secondary action, breathing

ÖZ

İŞBİRLİKÇİ ROBOTLARDA İNSAN-ROBOT ETKİLEŞİMİ DAVRANIŞI OLARAK "NEFES" ALIP VERME DAVRANIŞININ OLUŞTURULMASI VE ANALİZİ

Güneşdoğdu, Ali Nuri
Yüksek Lisans, Bilgisayar Mühendisliği Bölümü
Tez Yöneticisi: Doç. Dr. Erol Şahin
Ortak Tez Yöneticisi: Doç. Dr. Cengiz Acartürk

Ağustos 2022 , 69 sayfa

İşbirlikçi robotlar, sosyal insan-robot etkileşimi için yerleşik yetenekleri olmayan endüstriyel robot manipülatörleridir. Tezde, bir işbirlikçi robot üzerinde *ikincil eylem* animasyon ilkesinden esinlenerek *nefes* alıp vermeyi bir sosyal davranış olarak uyguladık. İnsan solunumundan ödünç alınan dalga biçimiyle otomatik olarak bir işbirlikçi robotun *nefes* alıp verme davranışını oluşturduk. Bu davranışın genliği ve frekansını parametre olarak kullandık.

Nefes davranışının parametrelerinin robot ve insanın ortak çalıştığı bir görev üzerindeki etkisini ölçmek için bir kullanıcı deneyi tasarladık. Çalışma sırasında, ortak görevin performansını değerlendirmek için görev tamamlama süresini ve görevin kalitesini değerlendirmek için deneklerin elinin hızlarını ve ivmelerini topladık. Kullanıcı anketini kullanarak insan-robot etkileşiminin kalitesini ölçtük. Topladığımız verilerin analizi, bir insanın nefes almasına benzer bir frekansın görev performansını olumlu yönde etkilediğini ve görev kalitesini iyileştirdiğini gösterdi; ancak, insan-robot et-

kileşimi kalitesini önemli ölçüde etkilemedi. Ayrıca, *nefes* davranışının genliğinin değiştirilmesi herhangi bir ölçümü etkilemedi.

Anahtar Kelimeler: İşbirlikçi robot, insan-robot etkileşimi, ikincil hareket, nefes

To beloved mom and dad

ACKNOWLEDGMENTS

This work was partially supported by TUBITAK with projects 120E269 and 117E002.

I wish to express my gratitude to my advisor Erol Şahin and Cengiz Acartürk for their invaluable support and guidance and for making me a member of the KOVAN family and for providing an excellent research environment and opportunities.

I am grateful to Hande Öğüt for her endless love, support, and encouragement.

Many thanks to my family and friends for being always there for me.

I owe special thanks to METU-ROMER (Center for Robotics and Artificial Intelligence) and its members for their support throughout this thesis.

TABLE OF CONTENTS

LIST OF TABLES

TABLES

LIST OF FIGURES

FIGURES

LIST OF ABBREVIATIONS

2D	2 Dimensional
3D	3 Dimensional
HRI	Human-Robot Interaction
Cobot	Collaborative Robot
IFR	International Federation of Robotics
ROS	Robot Operating System
IMU	Inertial Measurement Unit

CHAPTER 1

INTRODUCTION

1.1 Problem Definition and Motivation

The first industrial robot, Unimate, was installed at General Motors in 1961. Since then, industrial robotics has been growing both in numbers and applications. The market for them has shown solid growth in the last decade. According to the World Robotics 2021 report [19], published by the International Federation of Robotics (IFR), as of 2020, around three million industrial robots were in operation, and the number is forecasted to reach 4.8 million by 2024. Two factors are contributing to that growth. The first is the increasing demand for industrial automation. The second is the emergence of a new breed of robots called collaborative robots, a.k.a cobots.

Cobots directly interact with humans, while industrial robots operate separately from them. Industrial robots tend to be big, heavy, and strong enough to carry heavier objects, making them a potential danger for humans. However, cobots are designed to cooperate with humans while ensuring safety [20, 21]. This collaboration between humans and cobots increases its level from operating side by side to responding in real-time to the humans' actions while cooperating on the same part [20].

With the increasing level of collaboration, cobots are on their way to becoming workmates with humans; thus, they are expected to interact socially with humans to enable seamless collaboration [22, 23]. Despite not having any support for social human-robot interaction (HRI), their social capabilities can be improved.

In this thesis, we implemented a breathing-like behavior to improve the social HRI capability of a commercial cobot with no support for social HRI. We parametrized the

behavior as amplitude and frequency. We aimed to measure the effect of the behavior on task performance, task quality, and HRI quality under these changing parameters with a user study.

1.2 Contributions and Novelties

Our contributions are as follows:

- The implementation and parametrization of the breathing-like behavior for a cobot
- The empirical understanding of the effect of breathing-like behavior with different parameters on task performance, task quality, and HRI quality

1.3 The Outline of the Thesis

Chapter 2 reviews the literature on breathing behavior in animation and robotics studies. Chapter 3 explains the synthesis and implementation of breathing behavior on a cobot with its waveform generation and parametrization. Chapter 4 explains the experimental setup and measurements with their analyses. Chapter 5 includes a brief overview of the thesis and a discussion of the result.

CHAPTER 2

LITERATURE

This chapter presents literature on the general perspective of HRI of cobots, robotics, and animation studies to improve a character's social interaction capabilities, breathing studies from animations, and breathing used in HRI.

Human-robot interaction (HRI) is an interdisciplinary field that ranges from social robotics, which aims to create more sociable, socially intelligent, and socially interactive robots, to collaboration, which attempts to create safe, intuitive, and efficient interaction.

Villani et al., in their review [24], stated that the most research on the HRI of cobots studies two main challenges: safe collaboration, which aims to improve safety while increasing collaboration, and intuitive interfaces for programming robots, which aims to improve collaboration and facilitate the deployment of the cobot for new tasks. In general, these two challenges are driven by the objective of increasing efficiency. However, in the HRI of cobots, efficiency may not have the utmost importance for users [25]. The cognitive burden and mental stress induced by close interaction with cobots can also be problematic. To overcome this problem, a human-centered design based on human perception is recommended [24].

Humans' perception of a robot can be affected by its functionality, behaviors, or appearance. An erroneous design leads to an uncanny experience that increases the cognitive burden from the interaction.

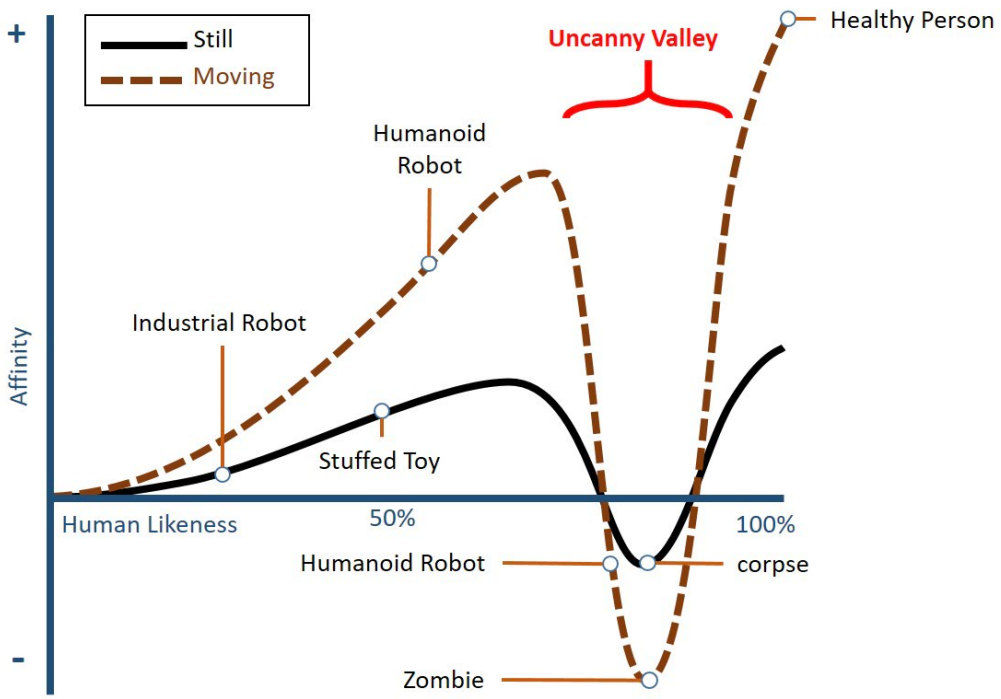

Figure 2.1: Uncanny Valley [1]

Mori [1] plots the graph between the similarity of an entity to humans and their affinity, as shown in Figure 2.1. He claims that an entity looked more human has more affection. A teddy bear has more affection than a cobot, as shown in Figure 2.2a and 2.2a. Further, he argues that human-like motion is more important than looking human-like to get human affection. The iCub, with human-like motion, such as waving its hand, has more affection than an ordinary teddy bear. He argues that this correlation is disturbed in some region he called the uncanny valley. In that region, humans' reactions towards a robot would abruptly shift from sympathy to eerie. The humanoid Sophia looks uncanny while iCub seems amiable, as shown in Figure 2.2. Mori suggested that a designer must avoid uncanny valley while designing a robot.

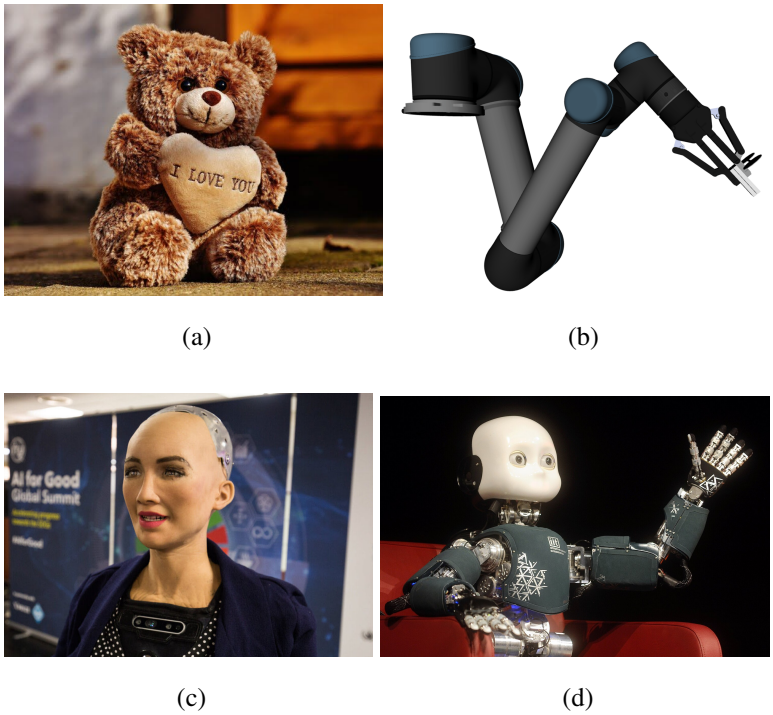

(a) (b)

(c) (d)

Figure 2.2: (a) An ordinary teddy bear, (b) A cobot, UR5, (c) The robot Sophia [2], (d) The robot iCub [3].

In Mori's graph, industrial robots have almost no affection from humans since they do not look or act like humans. They are designed as open-chain mechanisms for manipulation. Although their design is purely functional, adding human-like motions to them may increase their affection by giving them a more life-like character.

In the book "The Illusion of Life: Disney Animation" by Frank Thomas and Ollie Johnston [26], 12 essential principles shown in Figure 2.4 are proposed to make characters alive in cartoons. We are inspired by some of them in our study:

- *Appeal*

  The appeal is being visually attractive and interesting. Characters should have proper appeal for their expression. Humans love beautiful and gentle characters and dislike stiff and weird ones. By appeal, a character becomes alive. For example, a character on the right putting his hands in his pocket and whistling while walking is more appealing and alive than the character on the left in

Figure 2.3.

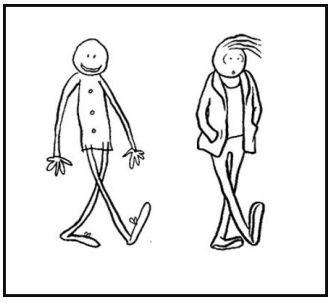

Figure 2.3: An appeal example [4]

- *Secondary Action*

  Secondary action is a motion that is not related to a character's intended actions or expressions but accompanies them. For example, humans always blink their eyes or breathe while doing their primary actions such as telling a story, working, or reading. Adding secondary actions similar to human behavior, such as breathing, contributes to a character's life-likeness.

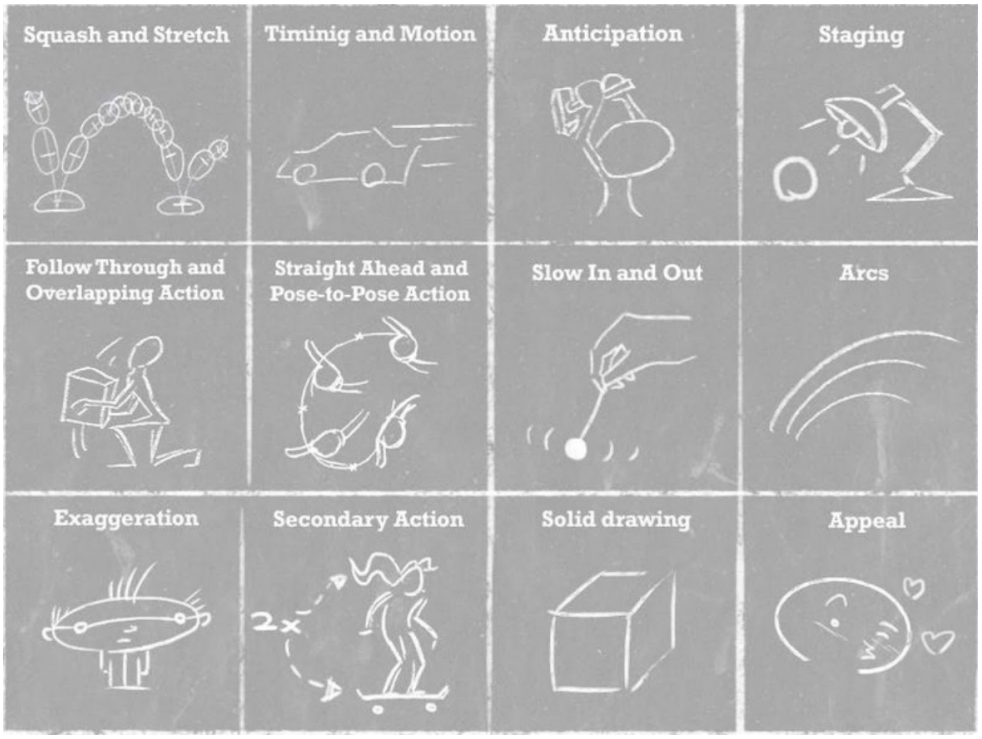

Figure 2.4: Animation Principles [5]

The principle of *secondary action* suggests that motion generated for a character can convince viewers that the character is alive similar to a moving entity can be more amiable for humans, as in Figure 2.1. It gives natural, human-like, and noticeable motion that makes a character alive to increase humans' affinity for the character. In secondary action, characters make unintended and unrelated actions, such as; playing with their hair or breathing, although their intended action is reading.

Some HRI studies [6, 7, 11, 13] adopted animation principles to give their robots a more pleasing appearance and natural, noticeable motions. Yohanan et al. and Bucci et al. [11, 13] used appealing stuffed animals and animal-like behaviors, like purring. Hoffman et al. and Terzioglu et al. [6, 7] designed their robots' behavior with an impression of a head. They used gaze gestures and secondary actions to increase the HRI quality.

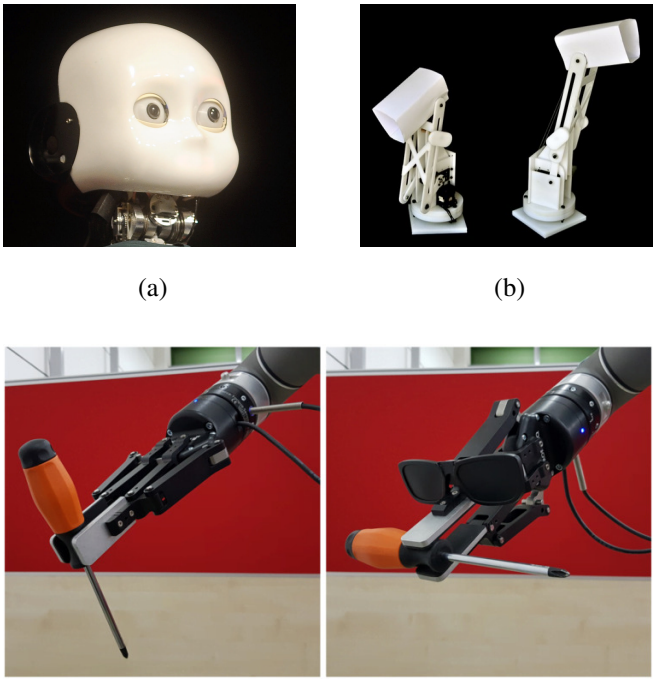

(a) (b)

(c)

Figure 2.5: Head Implementations: (a) The robot iCub [3], (b) Companion robot [6], (c) Uses an end-effector as head [7].

Riberio et al., [27] explored the possible use of animation principles in HRI and sug-

gested that breathing can be used as secondary action for robots, but they did not implement it. Hoffman et al. and Terzioglu et al. [6, 7] used breathing as secondary action. They only focused on breathing and non-breathing cases. They did not include parameters on their breathing behaviors.

In this thesis, we implemented a breathing-like behavior as a secondary action and parametrized it to investigate how these affect a cobot's collaboration and HRI capabilities.

2.1 Breathing

Breathing is the repetitive action of two main phases: inhaling and exhaling, that "moving air into and out of the lungs" in humans [28]. During breathing, the size of the trunk changes periodically, causing slight deformations in the chest and abdomen.

Humans generate breathing patterns that express various emotions [29] and correspond to arousal levels [30]. In a dangerous situation, humans respond to guarantee maximum respiration that yields rapid breathing. Tranquility is associated with slow breathing creating less deformation in the human's abdomen and chest [31].

Humans are perceptive to different breathing patterns and use them as nonverbal cues in their social interaction with others [29]. For example, a rapid breathing pattern could indicate a health problem.

Some HRI studies [7, 13, 16, 32] used breathing-like behaviors as nonverbal cues. Sefidgar et al. [32], and Terzioglu et al. [7] used *breathing* to affect humans' emotions and thoughts of a robot. They measured the difference between breathing and non-breathing conditions with user studies. They found that breathing significantly positively affects humans by decreasing anxiety. Additionally, Terzioglu et al. [7] found positive results in humans' feelings about robots, such as an increase in safety, intelligence, and sociability of robots. Humans thought the robot that was breathing was more enjoyable and likable.

Yohanan et al. [16], and Bucci et al. [13] used breathing to express the robot's levels of arousal and valance. They succeeded at expressing arousal but did not succeed

at expressing valance. They used the frequency of breathing to communicate the arousal, but the expression method of the valance differs between studies. Yohanan et al. [16] used the symmetry of breathing by adjusting the inhaling and exhaling time. Bucci et al. [13] used periodic and non-periodic breathing signals.

2.2 Creating Breathing-like Motion

The amplitude, frequency, and waveform of the signal driving the breathing-like motion must be chosen. [13].

Park et al. [10], Heloir et al. [33], Shapiro [34] implemented animation frameworks. They enable breathing animation as secondary action in their animation frameworks. They let designers decide what the waveform of breathing will be. Heloir et al. [33], and Shapiro [34] used simple models of the chest and abdomen. They generate breathing animation by enabling inflation of the chest and abdomen. Park et al. [10] used a complex skin model that induces skin deformations by a point cloud on the body. Breathing is generated using the motion of points in the point cloud.

Tsoli et al. [8], Zordan et al. [9] and Veltkamp et al. [35] simulated breathing. They generate accurate breathing simulations from given amplitude and frequency. They calculate the waveform of the breathing signal from their algorithms. Zordan et al. [9] and Veltkamp et al. [35] used muscle-tendon models to generate the waveform. Tsoli et al. [8] collected 3D scan data from 58 individuals' breathing to teach their model how to breathe. The model generates breathing simulations for 3D human avatars from real human respiration data measured by a respirometer.

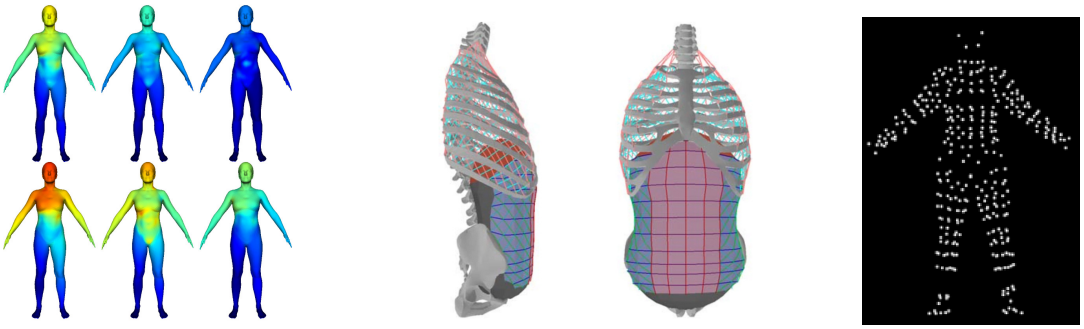

(a) (b) (c)

Figure 2.6: (a) Heat map that shows deformation of the human body while breathing [8]. (b) Tendon-muscle model used in breathing simulation in [9]. Green strings depict muscles that deform polygons to represent skin and deflect bones. (c) Point cloud from [10]. A designer can create breathing by adjusting the positions of points in the point cloud

Some robotics studies [11, 12, 13], as shown in Figure 2.7 had soft body surfaces that represented the belly of the creature, which enabled inflating and deflating with the motion of a servo motor to generate breathing.

(a) (b) (c)

Figure 2.7: Servo motor actuated breathing implementations: (a) Uses 4-bar mechanism [11] (b) Uses contraction and expansion of outer rings [12] (c) Uses artificial ribs that can open or close, shown as purple semi-circles [13]

Yoshida et al. [14], Asadi et al. [15], and Klausen et al. [36] used pneumatic actuators

that inflated and deflated balloon-like structures to generate breathing.

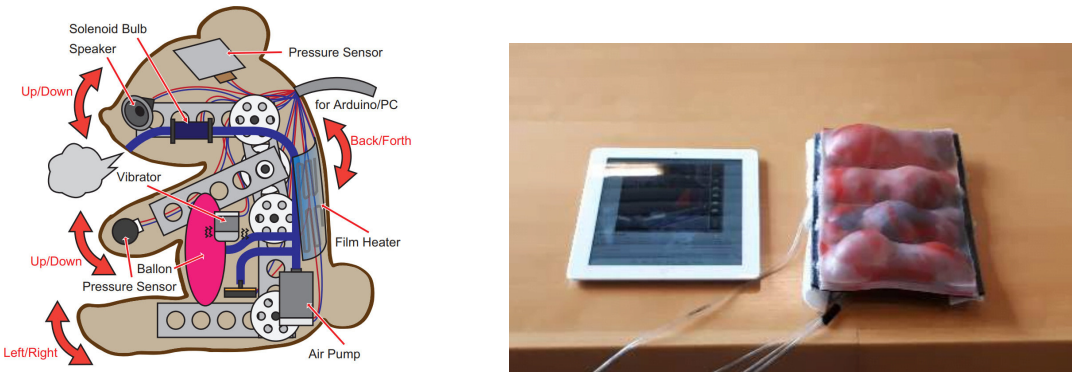

(a) (b)

Figure 2.8: Air actuated breathing implementations: (a) Uses a balloon and pump inside of a teddy bear [14]. (b) A soft robot designed as a balloon [15].

Hoffman et al.[6], and Terzioglu et al. [7] used independent head and body parts so that the body part performed the breathing behavior while the head did not contribute to the breathing behavior.

Basic sinusoidal waveforms are often used in the literature [6, 7, 10, 11, 12, 13, 14, 15, 16, 32, 33, 34, 36, 37, 38]. Yohanan et al., Sefidgar et al., and Ksie et al. [16, 32, 38] also used non-sinusoidal waveforms to express emotions, not to increase accuracy. Tsoli et al. [8], Zordan et al. [9] and Veltkamp et al. [35] used different waveforms to simulate breathing accurately, but neither of their solutions is applied to robots.

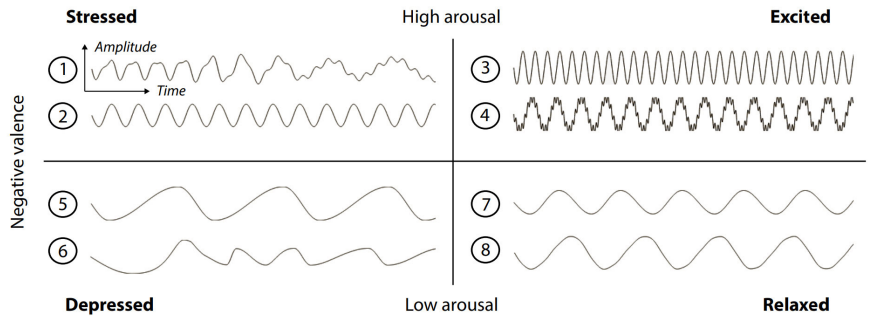

(a)

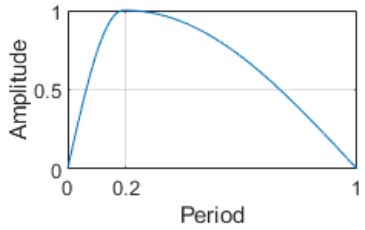

(b)

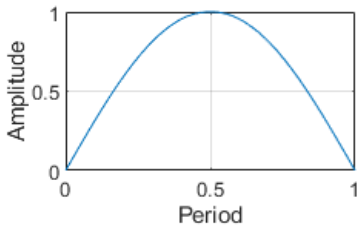

(c)

Figure 2.9: (a) Breathing waveforms from [13] (b) Asymmetrical breath pattern from [16] for expressing negative valance. (c) Symmetrical breath pattern from [16] for expressing positive valance.

In this thesis, we implemented a breathing waveform that is more accurate than a basic sinusoidal waveform using respiration data collected from a respirometer [17] since sinusoidal waveform can not cover all features of breathing [8].

CHAPTER 3

METHODOLOGY

In this chapter, we described the UR5 cobot platform on which we conducted this work and the generation and parametrization of *breathing* on it. Our generated breathing behavior is a reciprocal motion inspired by actual human breathing. The link between them is assumed. Calling actual breathing to our generated behavior requires more user studies and in-depth analysis. During this chapter, *breathing* refers to "breathing-like animation" behavior.

3.1 The UR5 Cobot Platform

We implemented *breathing* on a commercial cobot platform shown in Figure 3.1, a UR5 robotic manipulator (Universal Robots, Odense, Denmark) equipped with a 2F-140 two-finger gripper (Robotiq, Lévis, Canada). The UR5 has six joints: base, shoulder, elbow, and wrist 1-2-3. as shown in Figure 3.2

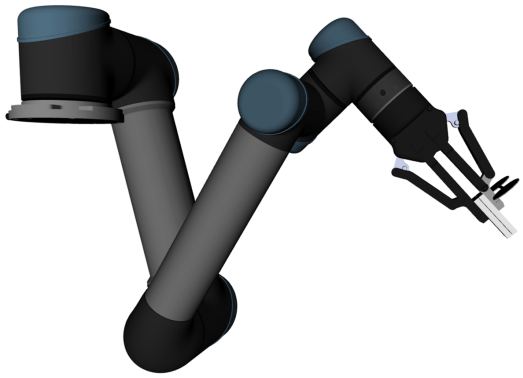

Figure 3.1: The UR5 cobot that is equipped with two finger gripper from Robotiq that sunglasses is affixed to

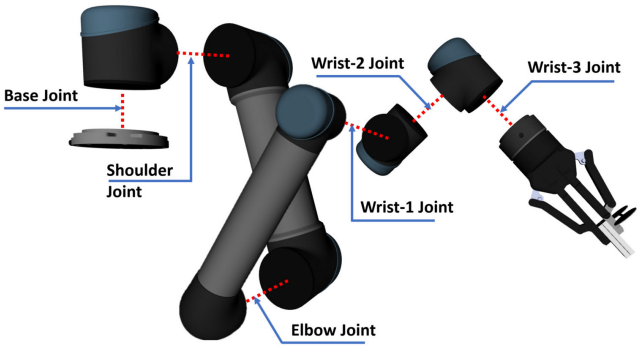

Figure 3.2: Joint names of the UR5

Terzioglu et al. [7] affixed a pair of sunglasses on the gripper to illustrate eyes and changed the gripper's default orientation to mimic a beak/mouth that create the impression of a head. We kept these additions since they improved the *Appeal* and boosted the HRI quality of the robot by contributing to its life-likeness [7].

We split the UR5 such three joints (wrist 1-2-3) of UR5 as neck joints to emphasize the impression of the head, and the remaining three joints (base, shoulder, and elbow) as body joints (see Figure 3.3). Neck joints control the head's orientation, while body joints control the head's position and create breathing.

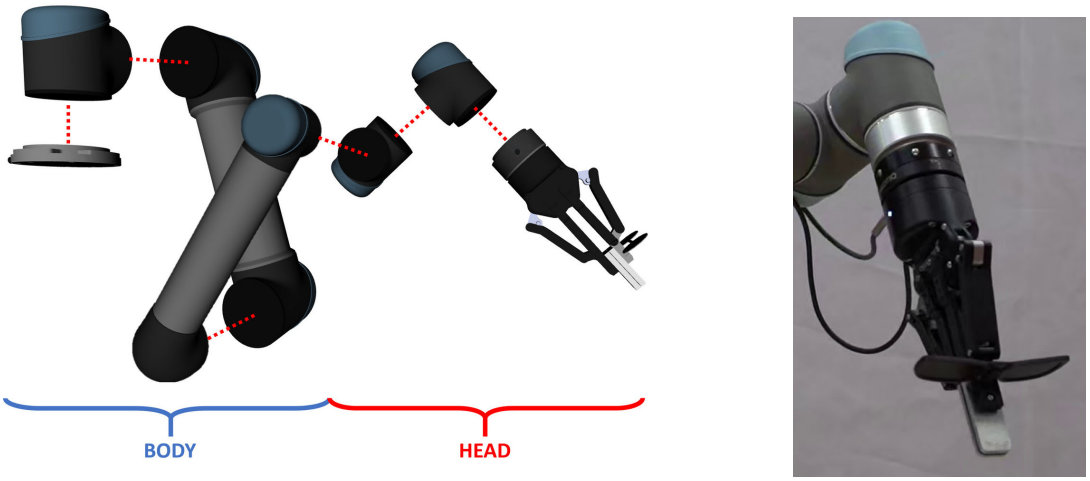

(a) (b)

Figure 3.3: (a) The UR5 joints split into *head* and *body* groups, (b) Head animation with two finger gripper from Robotiq that sunglasses is affixed to.

3.2 Breathing Concepts

We considered two options for creating an illusion of volume change since the UR5 is a robot composed of rigid body links and cannot alter the volume of its body: (1) The body is in an imaginary ellipsoid that its volume is changing while the body of the UR5 is stretching it by breathing, which is highly imaginary (2) Use of perspective such that while breathing, as body links are getting closer, they look bigger, but humans will probably guess that the effect comes from perspective. We abandoned these options since they are hypothetical about human perception.

We implemented breathing as a reciprocal body motion that causes the head to move around, which is similar to Hoffman et al. [6] and Terzioglu et al. [7] since breathing also creates small motions on the human chest [39]. The effect of human breathing is very small that direct use on the UR5 will not be noticeable. We use larger amplitude to make it noticeable. Our implementation used the volumetric change of air as a waveform, which is calculated by applying Euler integration on measured volumetric flow rate data from Nishi [17] plotted on Figure 3.4.

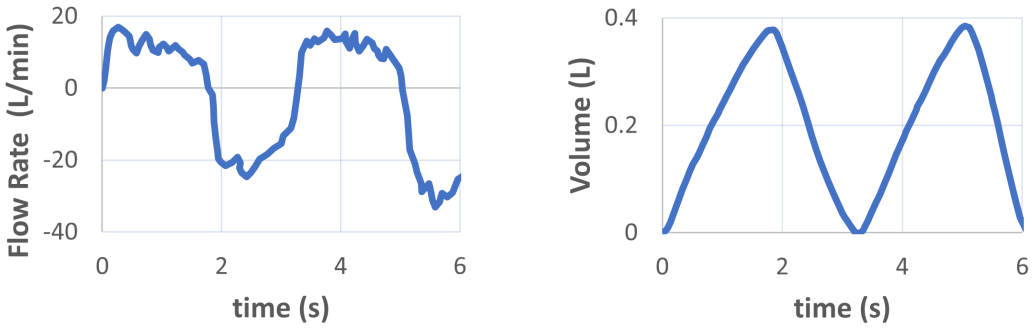

(a) (b)

Figure 3.4: (a) Volumetric flow rate of human breathing retrieved from [17], (b) Volume-time graph of human breathing obtained by integrating the volumetric flow rate data in (a).

The volumetric change of air is a time-series data represented by the tuple $V = (t, V_t)$ of a time and a value, where V_t is volume change value at time t. We create a param-

eterized breathing signal B from the volumetric change of air:

$$B_{tk_f} = k_a V_t \tag{3.1}$$

where k_a is the amplitude constant, k_f is the frequency constant, and V_t is the volumetric change of air used in a human's breathing. This maps the volumetric change of air V_t at time t to signal value B_{tk_f} at time tk_f by k_a. (See Figure 3.5 for examples.)

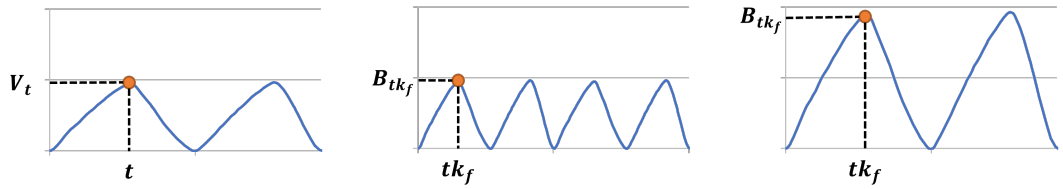

(a) (b) (c)

Figure 3.5: Parametrization examples of breathing signal. (a) Volume signal from Figure 3.4, (b) Breathing signal where $k_f = 0.5$ and $k_a = 1$, (c) Breathing signal where $k_f = 1$ and $k_a = 2$

3.3 Breathing Implementation

The UR5 animated breathing by moving its head along a direction represented by vector v_{breath}. The direction vector v_{breath} has two components in space as shown in Figure 3.6). They are up and forward, which is similar to human chest motion. Using the breathing signal, a trajectory is generated on this vector which is represented by a sequence of waypoints for the head position. The position of each waypoint is denoted as p_t, which is the position value of the head at time t and calculated as:

$$p_t = p_i + B_t v_{breath} \tag{3.2}$$

where B_t is the breathing signal at time t, v_{breath} is the direction vector, and p_i the initial position.

While changing the position p of the head, the orientation $o(v_{gaze})$ of it was kept constant during breathing. It helps avoid gestures, such as head shake, head nod, etc., and decreases the complexity of the motion for humans.

The pose q_t at time t is a concatenation of positions p_t at time t and the orientation $o(v_{gaze})$:

$$q_t = (p_t, o(v_{gaze})) \tag{3.3}$$

where orientation $o(v_{gaze})$ is calculated from the gaze vector v_{gaze}

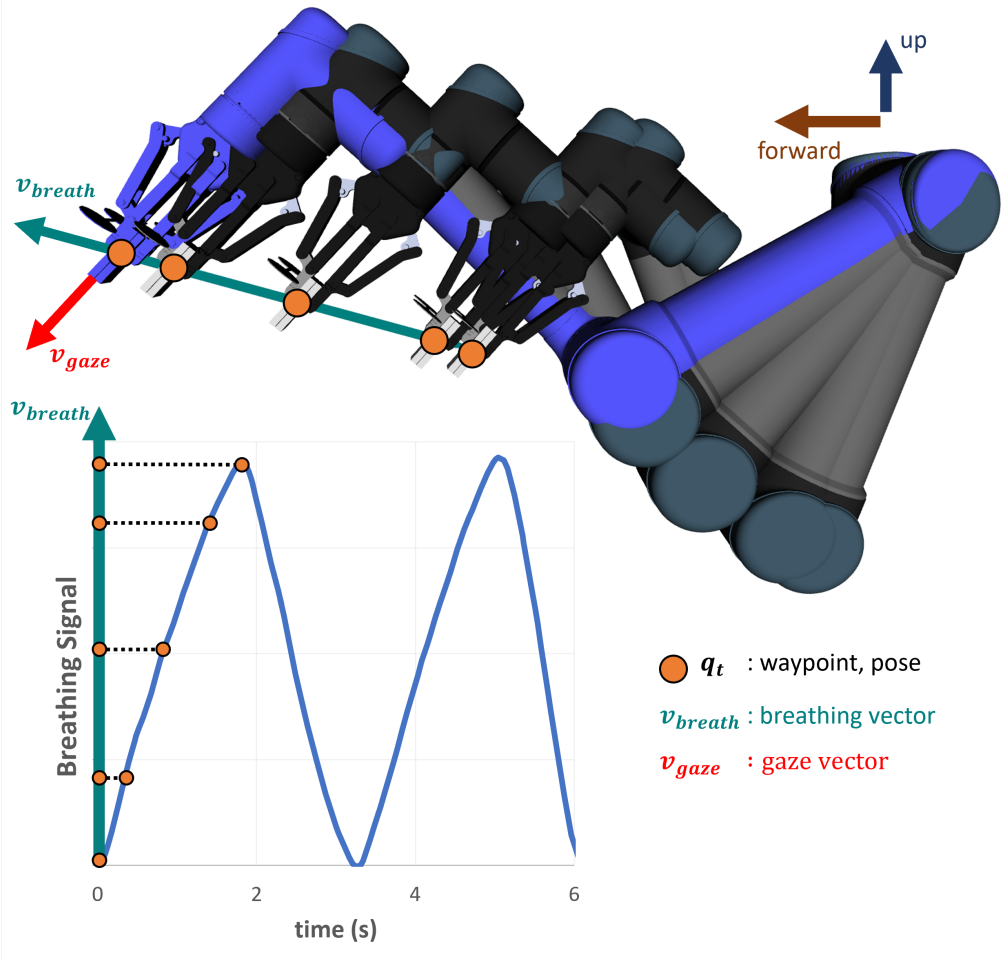

Figure 3.6: Orange circles represent waypoints of the trajectory. Every waypoint calculated as a pose q_t at time t by the breathing signal B_t, breathing vector v_{breath}, and gaze vector v_{gaze}. (See Equations 3.2 and 3.3)

The joint trajectory j_t at time t is calculated by inverse kinematic function:

$$j_t = IK(q_t) \tag{3.4}$$

where q_t is the pose at time t and $IK()$ is the inverse kinematic function.

The wrist-3 link of the UR5, which is represented by frame $\{6\}$ (see Figure 3.7 and 3.2), is redundant in the above inverse kinematic problem since z_6, z_5, and v_{gaze} are the same vectors.

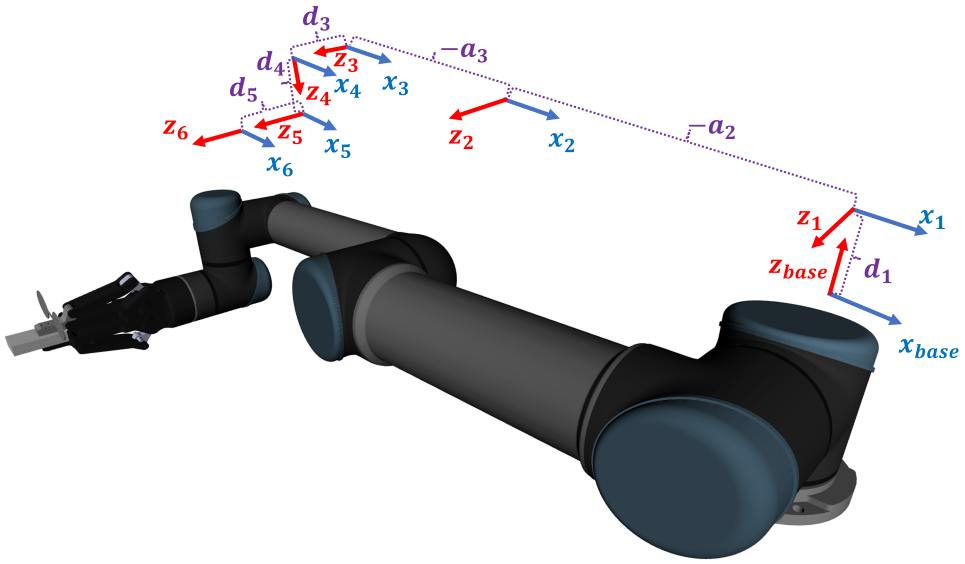

Figure 3.7: Coordinate frames on UR5. Each link of UR5 has its coordinate frame represented by $\{\text{n}\}$ and unit vectors of frames are represented by x_n, y_n, and z_n where n is the frame number. The $\{base\}$ coincides with the world coordinate frame. v_{gaze} is the same vector with z_6 and z_5.

Preserving the joint angle of wrist-3 causes head-tilt gesture [40]. To avoid it, the sunglasses on the gripper must be kept horizontal. Coordinate frame $\{6\}$ denotes the wrist-3 link. Axis x_6 is parallel to sunglasses and perpendicular with z_{base} since it must be parallel to the horizontal plane:

$$x_6 \cdot z_{base} = 0 \tag{3.5}$$

For ease of further calculations, all vectors are transformed into the frame $\{5\}$:

$$z_{base}^{5} = T_{base}^{5} z_{base} \tag{3.6}$$

$$x_{6}^{5} = T_{6}^{5} x_{6} \tag{3.7}$$

where z_{base}^{5} is the representation of the unit vector on z axis of the base frame $\{base\}$ in the fifth frame $\{5\}$, x_{6}^{5} is the representation of the unit vector on x axis of the sixth frame $\{6\}$ in the fifth frame $\{5\}$, T_{base}^{5} is the transformation matrix from the base frame $\{base\}$ to the fifth frame $\{5\}$, and T_{6}^{5} is the transformation matrix from the base frame $\{6\}$ to the fifth frame $\{5\}$.

T_{base}^{5} can be calculated by forward kinematics of the robot's first 5 axes. This leads to the vector z_{base}^{5}:

$$z_{base}^{5} = \begin{bmatrix} a_1 \\ a_2 \\ a_3 \end{bmatrix} \tag{3.8}$$

where a_1, a_2, a_3 are constants.

The transformation matrix T_{6}^{5} is calculated as:

$$T_{6}^{5} = \begin{bmatrix} cos\theta_6 & sin\theta_6 & 0 \\ -sin\theta_6 & cos\theta_6 & 0 \\ 0 & 0 & 1 \end{bmatrix} \tag{3.9}$$

where θ_6 is the angle of the wrist-3 joint as shown in Figure 3.7

x_{6}^{5} is calculated as:

$$x_{6}^{5} = \begin{bmatrix} cos\theta_6 \\ -sin\theta_6 \\ 0 \end{bmatrix} \tag{3.10}$$

by using Equation 3.7 and where x_6 is as:

$$x_6 = \begin{bmatrix} 1 \\ 0 \\ 0 \end{bmatrix} \tag{3.11}$$

Equations 3.5 is rewritten by Equations 3.8, and 3.10 as:

$$0 = a_1 cos\theta_6 - a_2 sin\theta_6 \tag{3.12}$$

Equation 3.12 has two solutions for θ_6. The main difference between them is the direction of the y_6 axis. It has to have a positive z side of the plane. This leads to inequality:

$$y_6 \cdot z_{base} > 0 \tag{3.13}$$

where y_6^5 is calculated as:

$$y_6^5 = T_6^5 y_6 \tag{3.14}$$

where T_6^5 is in equation 3.9, and y_6 is:

$$y_6 = \begin{bmatrix} 0 \\ 1 \\ 0 \end{bmatrix} \tag{3.15}$$

which yields to:

$$y_6^5 = \begin{bmatrix} sin\theta_6 \\ cos\theta_6 \\ 0 \end{bmatrix} \tag{3.16}$$

The inequality 3.13 is rewritten on θ_6 as:

$$0 < a_1 sin\theta_6 + a_2 cos\theta_6 \tag{3.17}$$

One of two solutions from Equation 3.12 must hold inequality 3.17. Thus, the angle of the wrist-3 joint is calculated for every waypoint.

CHAPTER 4

EXPERIMENTS AND RESULTS

4.1 Experimental Setup

The experimental setup consists of the UR5 cobot, a control computer running Ubuntu 16.04 image with Robot Operating System (ROS) [41] installation, a smartwatch, a webcam, and a task assembly, as shown in Figure 4.1.

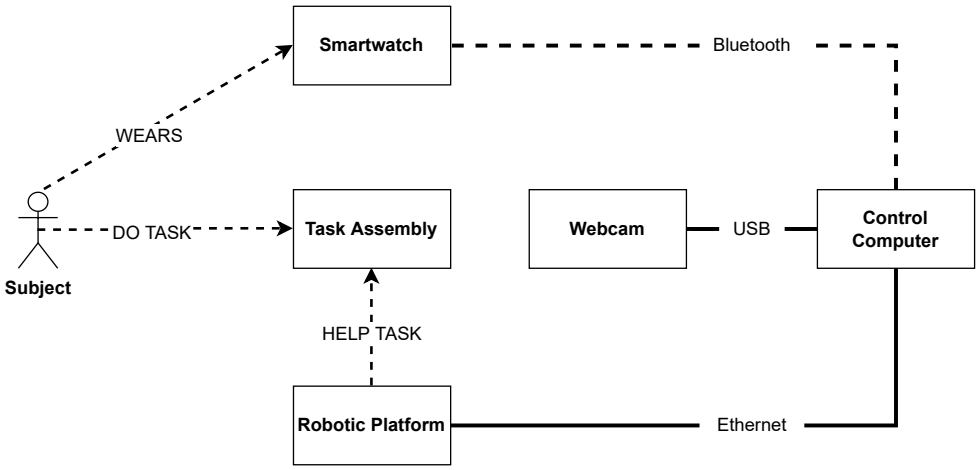

Figure 4.1: Experimental Framework

4.1.1 Experimental Setting

The experimental setting includes a test robot, "UR5", a table, and a chair. (see in Figure 4.2). The table is a shared workspace between the subject and UR5. The chair is for the subject to sit during the experiment.

Figure 4.2: The experimental setup with a subject

4.1.2 Smartwatch

The smartwatch, as shown in Figure 4.3, has a Bluetooth communication module and a 9-axis inertial measurement unit (IMU). In the experiment, a custom application collects data from the IMU module that measures the angular speed and linear acceleration of the hand of the subject and sends them to the control computer via Bluetooth.

Figure 4.3: Smartwatch, retrieved from [18]

4.1.3 Control Computer and Webcam

The control computer has Bluetooth, an ethernet socket, and a USB input. The ethernet socket connects the robot and gripper to the control computer. The control computer is also connected to a webcam via USB that helps follow the experiment and the subject.

4.1.4 Task Assembly

Task assembly consists of a 3D printed bolt holder, a 3D printed screw holder, three screws "$M8 \times 35$", a bolt "$M8$", and two boxes as shown in Figure 4.4. The bolt holder has a handle and is affixed to the table.

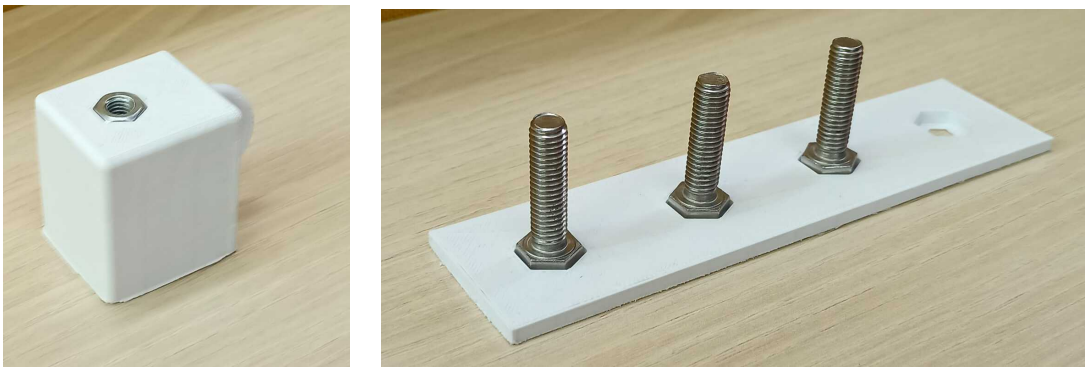

(a) (b)

Figure 4.4: (a) The bolt holder with a bolt attached, (b) the screw holder with three screws.

4.2 Collaborative Task in the Study

The collaborative task is a quality control task that is the inspection of newly manufactured screws. Screws are provided in the screw holders. The robot's task is to deliver screws to the subject. The subject's task is to inspect their quality. The robot performs breathing while the subject is inspecting a screw.

The collaborative task in this study is a sequential collaborative task [20] where a human and a robot work together in the workspace, but their movements are sequential. While the human works on the task, the robot waits.

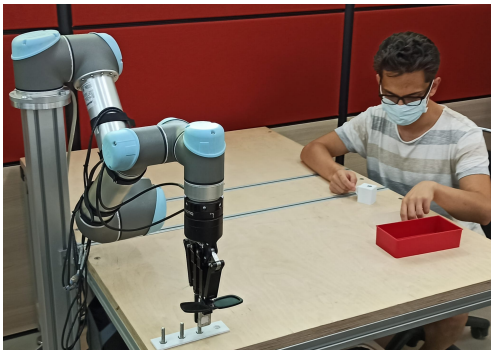

(a)

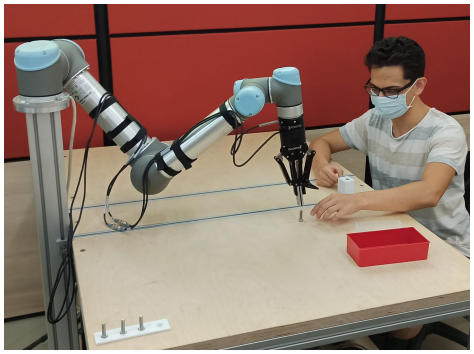

(b)

(c)

Figure 4.5: The collaborative task (a) The robot takes a screw from the screw holder (b) The robot delivers a screw to the subject (c) The robot is in the idle state, breathing and waiting for the subject to finish the inspection of the screw

The robot has two states: *breathing*, where it waits for the human to work, and *working* as shown in Figure 4.6. During the *breathing* state, the robot executes breathing. When the human finishes work, the robot switches to the *working* state in which the robot performs its part of the collaborative task. The robot does not perform breathing action in *working* state since breathing is treated as a secondary action. Breathing during *working* state would make it primary action attracting participants' attention.

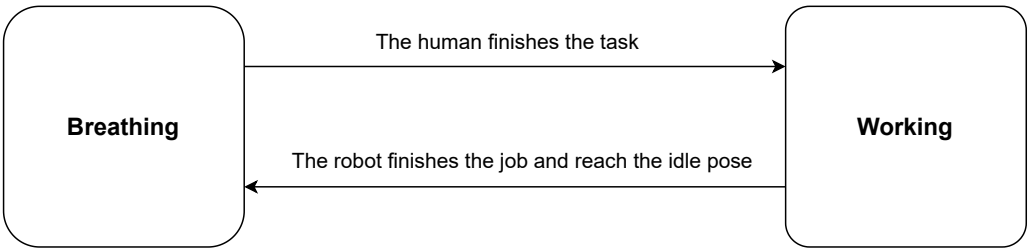

Figure 4.6: The state diagram of the robot in the collaborative task

The quality inspection is completed by mounting and dismounting screws on the bolt. Screw mounting must be smooth for high-quality screws. Subjects inspect by the feeling in their hand. If they feel any abrasion, discontinuity, or surface roughness implies the screw has manufacturing defects. Screw with high quality and defects goes different boxes. Each trial includes a quality inspection of one screw. The same set of 3 screws was used during the experiment, and all of them were high-quality screws.

4.3 Experimental Method

The experiment has two within-subject parameters: amplitude and frequency. Three unique conditions are created to test these parameters: *Control*, *Larger Amplitude*, and *Higher Frequency*. A frequency of 20 breaths per minute (bpm) close to human breathing frequency was chosen as the control condition frequency, and smaller amplitude of 5 cm displacement was selected as the control condition amplitude.

The larger amplitude condition was used to test the amplitude parameter, and a larger amplitude of 10 cm displacement was selected as amplitude, while the frequency was kept the same as the control condition.

The higher frequency condition was to test the frequency parameter, and a higher frequency of 40 bpm was selected as the frequency, while the amplitude was kept the same as the control condition.

Every participant was exposed to all conditions. The control condition is repeated to curtail carry-over effects. Thus, every participant was exposed to a total of four

experimental conditions. Each condition has three trials. After every three trials, subjects filled the Godspeed Questionnaire [42]. In order to reduce ordering effects, we created four random ordering patterns, as shown in Figure 4.7

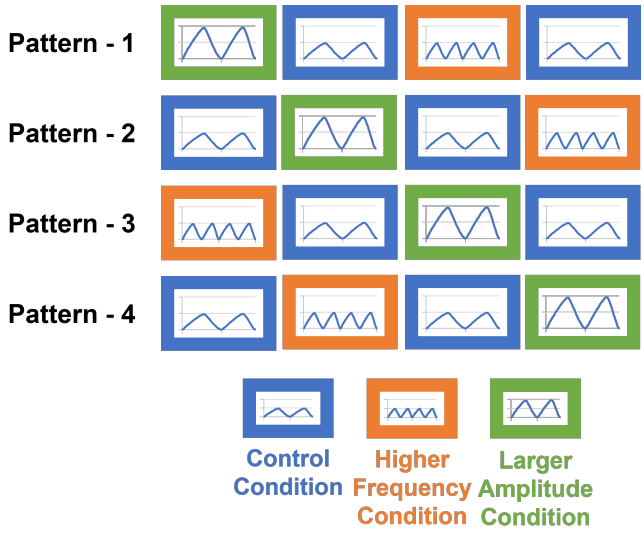

Figure 4.7: Randomized breathing ordering patterns used in the study.

4.3.1 Experiment Flow

The experiment starts with a briefing about the procedure and details of the task. In the briefing, subjects experience the screwing task and observe the action of pick and place of the robot, though they do not see the breathing. After the briefing, the experiment starts with the action of pick and place of the robot. After three trials experimenter gives the questionnaire to the subject and waits for the subject to finish it, this process is repeated until the subject is exposed to four conditions. The flow chart of the experiment is shown in Figure 4.8.

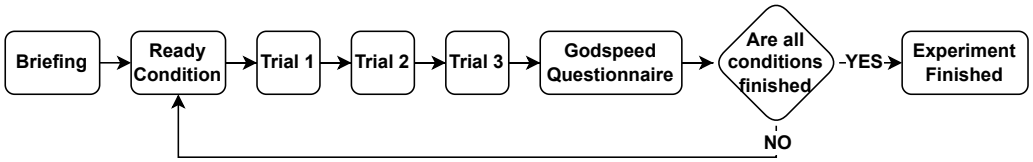

Figure 4.8: Experiment flow chart.

4.3.2 Trial Flow

The experimenter starts the trial by starting the robot then the experimenter starts monitoring the subject to detect the completion of the task. The robot picks a screw and delivers it to the table. After conveying the screw, the robot starts to perform breathing with specified parameters. With the screw delivered to the table, the subject picks the screw and starts quality control of the screw. After finishing the quality control, the subject puts the screw into the appropriate box. When the experimenter sees the screw in a box, the experimenter intercepts the robot. The robot stops breathing that finishes the trial. During trials, the same three screws are used for simplicity, despite subjects being told that the screws are renewed at all trials. The flow chart of a trial is shown in Figure 4.9.

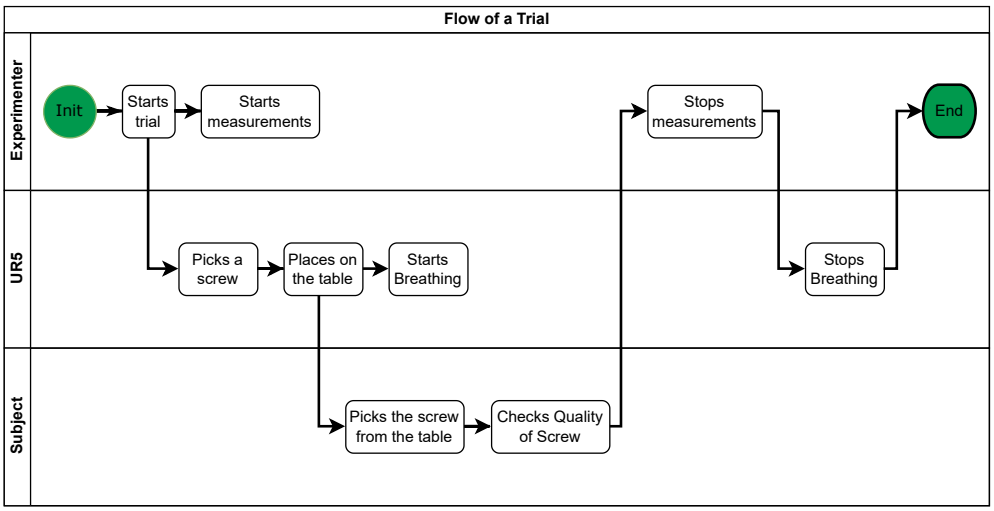

Figure 4.9: Experiment flow chart.

4.3.3 Measurements

We measure:

- Task Performance
- Task Quality
- HRI Quality

4.3.3.1 Task performance

Task performance is evaluated by the task completion times of participants. Higher task completion time corresponds to poor task performance. The task completion time t_c is calculated as:

$$t_c = t_f - t_s \tag{4.1}$$

where t_s is starting time when a participant takes the screw, and t_f is the finishing time when a participant puts the screw on the box. The experimenter recorded the t_s and t_f by taking timestamps from the control computer.

4.3.3.2 Task Quality

Task quality is evaluated by the angular speed and linear acceleration of participants' hands during a trial. Higher acceleration and speed data correspond to poor task quality. The data was collected via the smartwatch and recorded on the control computer. The recorded data is raw accelerometer and gyroscope readings from the IMU.

4.3.3.3 HRI Quality

We used the Godspeed questionnaire [42] to evaluate HRI quality. The Godspeed questionnaire uses the semantic differential method to evaluate five aspects:

- Anthropomorphism: This aspect refers to how much resemblance non-human entities such as robots have with human-like traits.
- Animacy: This aspect refers to how much a robot can imitate the authenticity of life.
- Likeability: This aspect refers to the stimulation of positive sensations of a robot on humans.
- Perceived Intelligence: This aspect refers to a criterion of how humans discern a robot as an intelligent entity.

- Perceived Safety: This aspect refers to the combination of the amenity of working with the robot and the feeling of menace from the robot.

4.3.4 Participants

29 individuals (9 female, 20 male) with ages was ranging from 20 to 34 (M = 27.38, SD = 2.73) participated the experiment. The experiment lasted approximately 30 minutes for each participant. The experiment was held at Kovan Research Center in METU.

4.4 Data Analyses and Results

4.4.1 Task Performance Analyses and Results

The average task completion time of three trials is used as the measure. The results from the amplitude experiment condition $(M = 27.314, SD = 7.029)$ and the control condition $(M = 27.240, SD = 7.215)$ resulted with amplitude of the motion has no effect on task completion time, $t(28) = 0.140, p = .890$. Descriptive plots are shown in Figure 4.10.

The results from the frequency experiment condition (M = 29.621, SD = 7.929) and the control condition (M = 27.180, SD = 6.680) indicates that frequency of the motion has significant negative effect on task completion time, $t(28) = -3.263, p = .003$. With higher frequency motion, task completion time increases. Descriptive plots are shown in Figure 4.11.

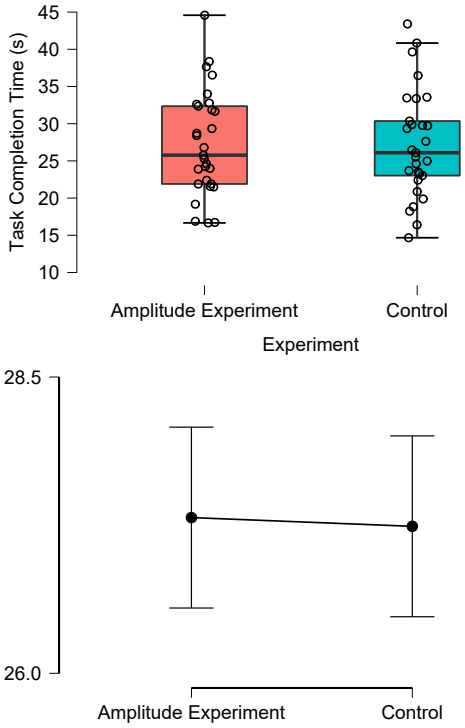

Figure 4.10: Task completion time results for amplitude experiment

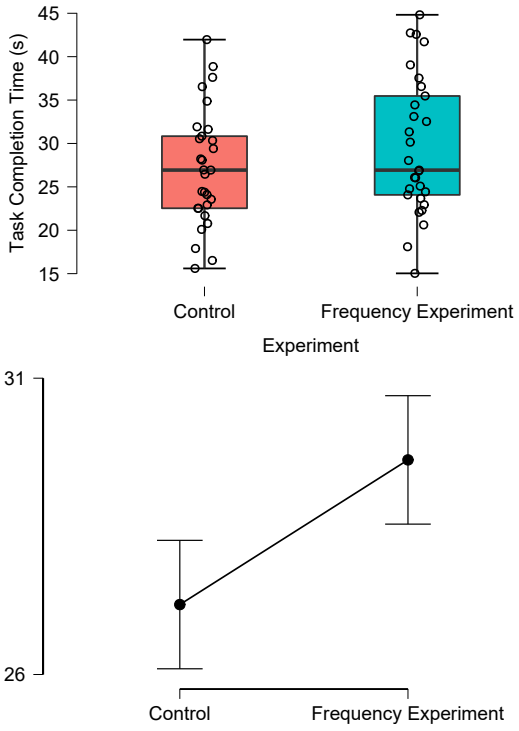

Figure 4.11: Task completion time results for frequency experiment

4.4.2 Task Quality Analyses and Results

We post-processed raw data to extract 6 features: mean, standard deviation, absolute mean, absolute standard deviation, absolute maximum, and maximum span.

Descriptive tables and figures are shown in Appendix B. Due to the high amount of data, paired t-test results are tabulated in 6 separate tables for every axis of raw data. (See Tables 4.1, 4.2, 4.3, 4.4, 4.5, and 4.6)

Table 4.1: Paired Samples T-Test of Angular Velocities at Axis 1

	Frequency Experiment			Amplitude Experiment		
	t	df	p	t	df	p
mean	-0.071	28	0.944	-0.663	28	0.512
standard deviation	0.611	28	0.545	1.597	28	0.121
absolute mean	1.026	28	0.313	1.161	28	0.255
absolute standard deviation	0.513	28	0.611	1.677	28	0.104
absolute maximum value	-0.486	28	0.630	0.833	28	0.411
max span	-0.428	28	0.671	0.988	28	0.331

Table 4.2: Paired Samples T-Test of Angular Velocities at Axis 2

	Frequency Experiment			Amplitude Experiment		
	t	df	p	t	df	p
mean	-0.275	28	0.785	1.429	28	0.164
standard deviation	-0.293	28	0.771	-0.862	28	0.396
absolute mean	-0.585	28	0.562	-0.316	28	0.754
absolute standard deviation	-0.219	28	0.828	-1.016	28	0.318
absolute maximum value	-0.585	28	0.563	0.2126	28	0.833
max span	-0.371	28	0.712	-0.1658	28	0.869

Table 4.3: Paired Samples T-Test of Angular Velocities at Axis 3

	Frequency Experiment			Amplitude Experiment		
	t	df	p	t	df	p
mean	−0.839	28	0.408	−1.364	28	0.183
standard deviation	0.956	28	0.347	−0.674	28	0.505
absolute mean	1.192	28	0.242	−0.815	28	0.421
absolute standard deviation	0.869	28	0.392	−0.606	28	0.549
absolute maximum value	0.023	28	0.981	−0.982	28	0.334
max span	0.370	28	0.713	−0.956	28	0.347

Table 4.4: Paired Samples T-Test of Linear Accelerations at Axis 1

	Frequency Experiment			Amplitude Experiment		
	t	df	p	t	df	p
mean	−0.133	28	0.894	0.170	28	0.866
standard deviation	−1.237	28	0.226	−0.720	28	0.477
absolute mean	−0.747	28	0.461	−0.652	28	0.519
absolute standard deviation	−1.860	28	0.073	−0.637	28	0.529
absolute maximum value	−2.174	28	0.038	1.389	28	0.175
max span	−2.279	28	0.030	1.127	28	0.269

Table 4.5: Paired Samples T-Test of Linear Accelerations at Axis 2

	Frequency Experiment			Amplitude Experiment		
	t	df	p	t	df	p
mean	0.083	28	0.934	−2.013	28	0.066
standard deviation	0.592	28	0.558	0.243	28	0.809
absolute mean	1.165	28	0.253	0.308	28	0.760
absolute standard deviation	0.051	28	0.959	0.212	28	0.833
absolute maximum value	−0.732	28	0.470	−1.026	28	0.313
max span	−1.199	28	0.240	−0.760	28	0.453

Table 4.6: Paired Samples T-Test of Linear Accelerations at Axis 3

	Frequency Experiment			Amplitude Experiment		
	t	df	p	t	df	p
mean	0.486	28	0.631	0.949	28	0.350
standard deviation	−1.486	28	0.148	0.360	28	0.721
absolute mean	−0.368	28	0.715	0.930	28	0.360
absolute standard deviation	−1.519	28	0.140	0.208	28	0.837
absolute maximum value	−1.612	28	0.118	0.112	28	0.911
max span	−1.658	28	0.108	0.223	28	0.825

The only significant results were on maximum span and absolute maximum features of linear acceleration at axis 1. For absolute maximum feature, the results from the frequency experiment condition (M = 0.114, SD = 0.047) and the control condition (M = 0.101, SD = 0.033) indicates that frequency of the motion has significant negative effect on task quality, $t(28) = -2.174, p = .038$. For maximum span feature, the results from the frequency experiment condition (M = 0.201, SD = 0.078) and the control condition (M = 0.180, SD = 0.058) indicates that frequency of the motion has significant negative effect on task quality, $t(28) = -2.279, p = .030$. Descriptive plots are shown in Figure 4.12.

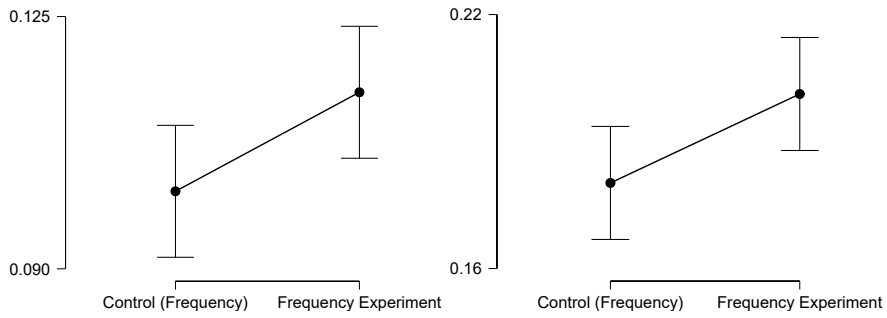

Figure 4.12: Results from the maximum span and absolute maximum features

4.4.3 HRI Quality Analyses and Results

Analyzing the Godspeed questionnaire requires Cronbach's a test to check the validity of the result. Results are assumed as valid when the value of Cronbach's a is higher than 0.7 [42]. For the amplitude experiment condition, the anthropomorphism sub-scale comprises 5 items $(a = .479)$, the animacy sub-scale comprises 6 items $(a = .853)$, the likeability sub-scale comprises 5 items $(a = .925)$, the perceived intelligence sub-scale comprises 5 items $(a = .865)$, the perceived safety sub-scale comprises 3 items $(a = .690)$. For the control condition, the anthropomorphism sub-scale comprises 5 items $(a = .549)$, the animacy sub-scale comprises 6 items $(a = .817)$, the likeability sub-scale comprises 5 items $(a = .943)$, the perceived intelligence sub-scale comprises 5 items $(a = .802)$, and the perceived safety sub-scale comprises 3 items $(a = .647)$. Descriptive plots are shown in Figure 4.13.

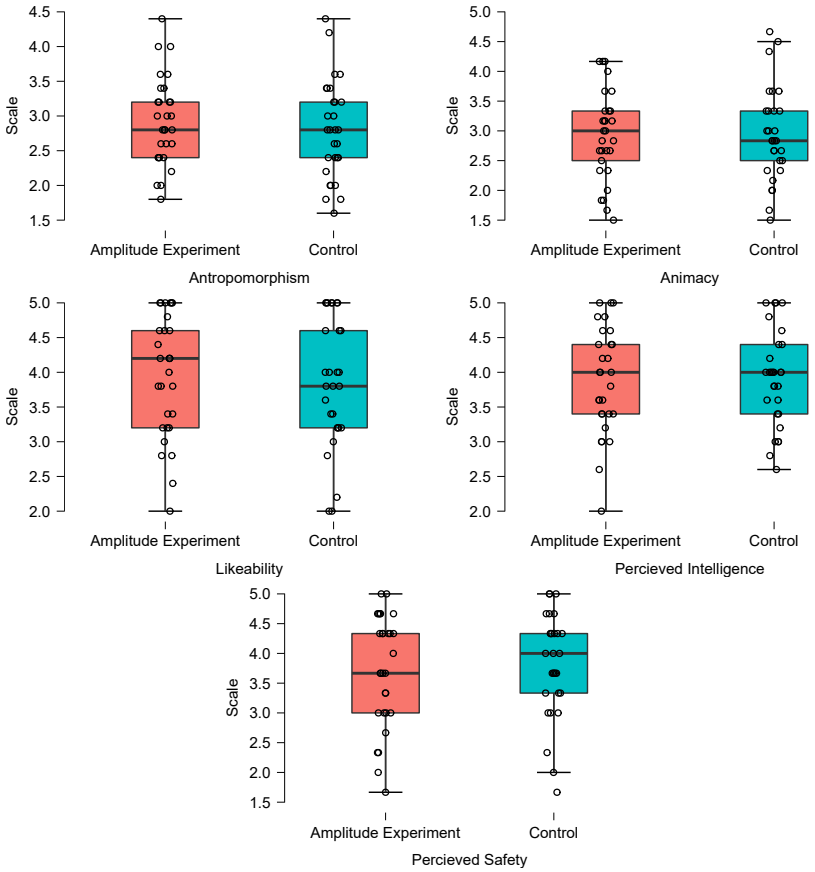

Figure 4.13: Godspeed questionnaire results for amplitude experiment

For the frequency experiment condition, the anthropomorphism sub-scale is consist of 5 items ($a = .744$), the animacy sub-scale is consist of 6 items ($a = .764$), the likeability sub-scale is consist of 5 items ($a = .925$), the perceived intelligence sub-scale is consist of 5 items ($a = .812$), the perceived safety sub-scale is consist of 3 items ($a = .412$). For the control condition, the anthropomorphism sub-scale is consist of 5 items ($a = .751$), the animacy sub-scale is consist of 6 items ($a = .783$), the likeability sub-scale is consist of 5 items ($a = .911$), the perceived intelligence sub-scale is consist of 5 items ($a = .841$), the perceived safety sub-scale is consist of 3 items ($a = .488$). The perceived safety sub-scale is not appropriate for further investigation since it is not valid for the frequency experiment. Descriptive plots are shown in Figure 4.14.

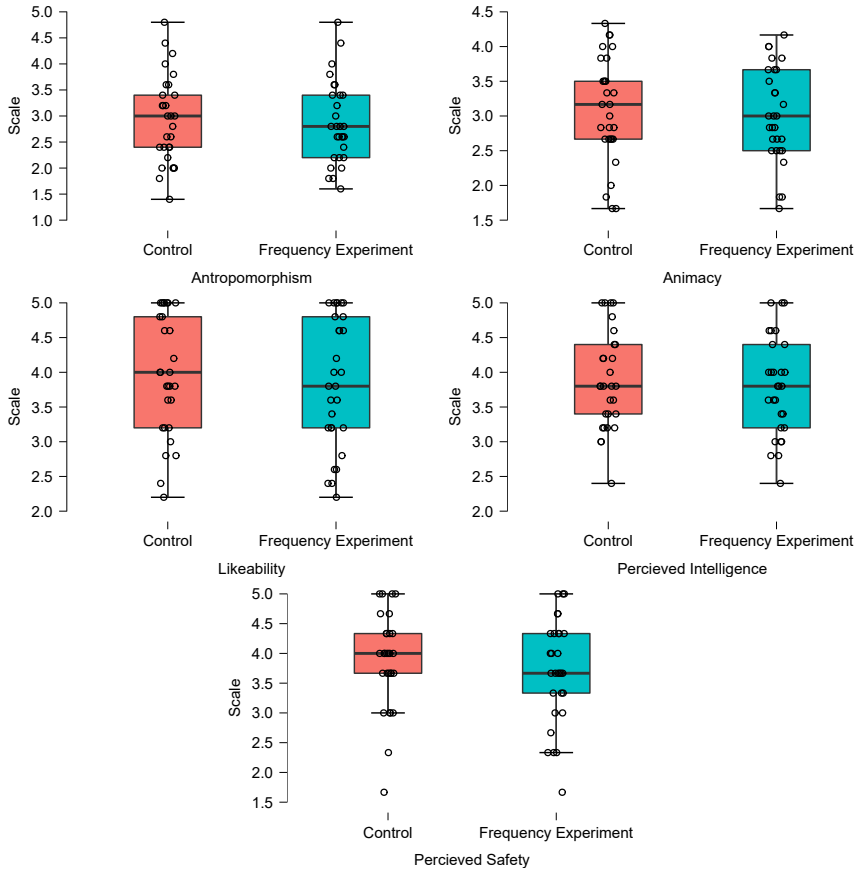

Figure 4.14: Godspeed questionnaire results for frequency experiment

4.4.3.1 Anthropomorphism

The anthropomorphism sub-scale for amplitude experiment condition ($M = 2.924, SD = 0.631$) is slightly higher than control condition ($M = 2.924, SD = 0.631$), where $t(28) = 1.512, p = .142$. However, the anthropomorphism sub-scale is invalid since it has low Cronbach's a. The anthropomorphism sub-scale for frequency experiment condition ($M = 2.862, SD = 0.793$) is very similar with the control condition ($M = 2.924, SD = 0.839$) , where $t(28) = 0.544, p = .591$. Descriptive plots are shown in Figure 4.15.

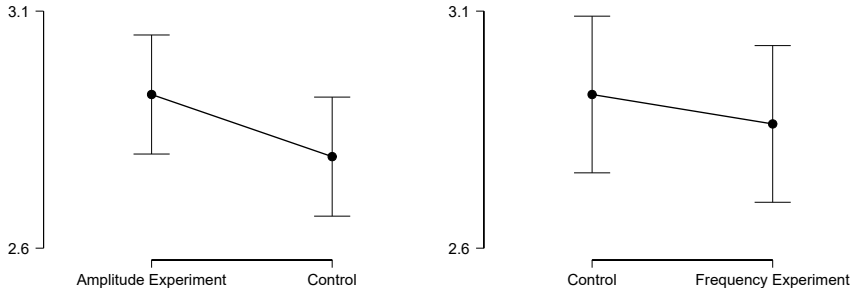

Figure 4.15: Descriptive plots for paired samples t-test of anthropomorphism sub-scales

4.4.3.2 Animacy

The animacy sub-scale for amplitude experiment condition ($M = 2.935, SD = 0.747$) is similar with control condition ($M = 2.937, SD = 0.780$), where $t(28) = -0.109, p = .914$. The animacy sub-scale for frequency experiment condition ($M = 3.011, SD = 0.680$) is slightly lower than the control condition ($M = 3.092, SD = 0.754$) , where $t(28) = -1.192, p = .243$. However, the difference is not significant. Descriptive plots are shown in Figure 4.16.

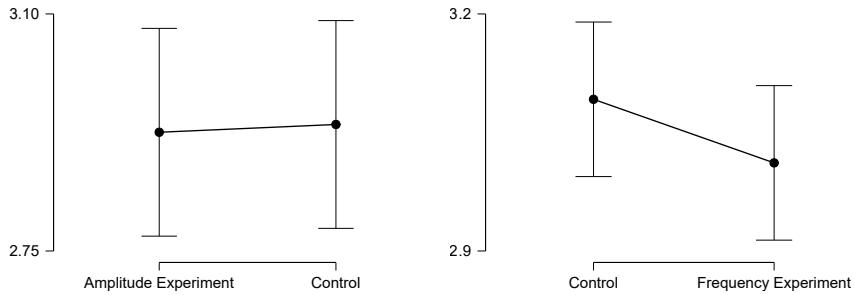

Figure 4.16: Descriptive plots for paired samples t-test of the animacy sub-scales

4.4.3.3 Likeability

The likeability sub-scale for amplitude experiment condition ($M = 3.952, SD = 0.870$)is slightly higher than control condition ($M = 3.841, SD = 0.937$), where $t(28) = 1.216, p = .234$. However, the difference is not significant. The likeability sub-scale for frequency experiment condition ($M = 3.848, SD = 0.942$) is slightly lower than the control condition ($M = 3.972, SD = 0.868$) , where $t(28) = -0.955, p = .348$. However, the difference is not significant. Descriptive plots are shown in Figure 4.17.

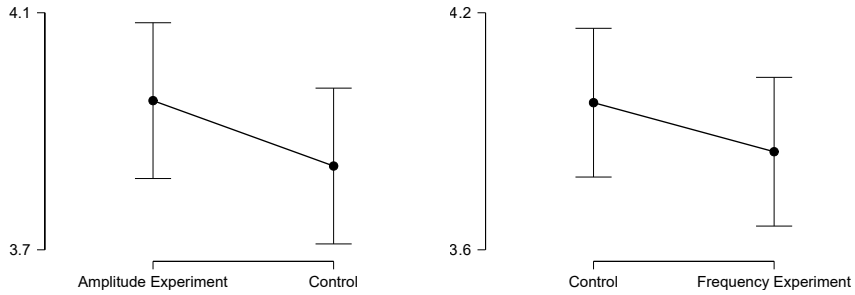

Figure 4.17: Descriptive plots for paired samples t-test of the likeability sub-scales

4.4.3.4 Perceived Intelligence

The perceived intelligence sub-scale for amplitude experiment condition ($M = 3.876, SD = 0.772$)is similar with the control condition ($M = 3.910, SD = 0.690$), where $t(28) = -0.391, p = .699$. The perceived intelligence sub-scale for frequency experiment condition ($M = 3.793, SD = 0.700$) is slightly lower than the control condition

$(M = 3.876, SD = 0.712)$, where $t(28) = -1.380, p = .179$. However, the difference is not significant. Descriptive plots are shown in Figure 4.18.

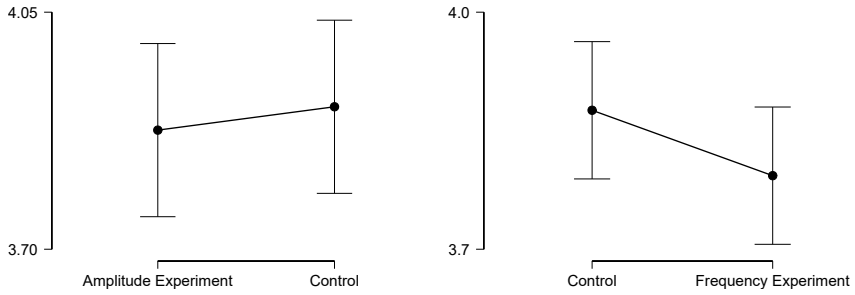

Figure 4.18: Descriptive plots for paired samples t-test of the perceived intelligence sub-scales

4.4.3.5 Perceived Safety

The perceived safety sub-scale for amplitude experiment condition $(M = 3.713, SD = 0.937)$is similar with the control condition $(M = 3.805, SD = 0.866)$, where $t(28) = -0.859, p = .398$. However, the perceived safety sub-scale is invalid since it has a low Cronbach's a. The perceived safety sub-scale for frequency experiment condition $(M = 3.701, SD = 0.874)$ is slightly lower than the control condition $(M = 3.885, SD = 0.798)$, where $t(28) = -1.417, p = .168$. However, the difference is insignificant, and the perceived safety sub-scale is invalid since it has a low Cronbach's a. Descriptive plots are shown in Figure 4.19.

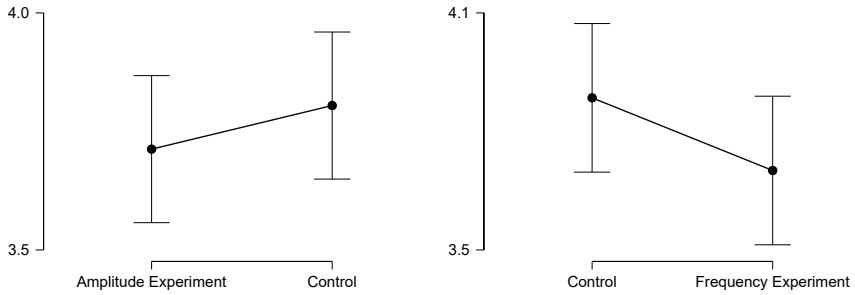

Figure 4.19: Descriptive plots for paired samples t-test of the perceived safety sub-scales

CHAPTER 5

DISCUSSION AND CONCLUSION

In this thesis, we developed a breathing-like repetitive motion for a cobot as a social behavior inspired by the *secondary action* animation principle to improve cobots' social HRI capabilities. We called this motion *breathing*; however, we are aware that classifying the generated motion as actual breathing will be inappropriate as there are endless possible motions that imitate breathing, and classifying them as breathing requires more user studies and in-depth analysis of them.

We used a breathing signal to implement *breathing* with its waveform recorded from human breathing with two parameters: *frequency* and *amplitude*. We test below two hypotheses generated from the parameters with a user study:

- The breathing behavior with similar frequency to humans will increase task performance, task quality, and HRI quality.
- As breathing amplitude increases, task performance, task quality, and HRI quality will decrease.

We designed our experiment to individually correct each hypothesis. We create two test conditions: larger amplitude and higher frequency, and a control condition to test against. We applied the control condition to each test condition to eliminate carry-over effects and evaluated their results by paired sample t-tests.

In this thesis, we evaluated task performance by task completion time, task quality by velocities and accelerations of the user's hand, and HRI quality by the Godspeed questionnaire [42] at Appendix A. The analysis of collected data showed that a frequency similar to a human's breathing positively impacts task performance by de-

creasing the completion time significantly and task quality by reducing the amplitude of acceleration of participants' hands.

The HRI quality result showed a consistently positive effect for a frequency similar to a human's breathing; however, it did not show any significance. Their only significant result is perceived safety, with the third adjective pair removed from the Godspeed questionnaire. Significance is diminished when the third adjective pair is kept in the analysis.

We expected the larger amplitude to disrupt user comfort and affect our result. However, the second hypothesis is negated by participants not being affected by the change of the amplitude of the *breathing*.

Negation of our hypothesis on HRI quality might be the result of the smaller amplitude we applied not attracting enough attention from participants; however, increasing the amplitude might attract too much attention; thus, might be violated our implementation of secondary action.

We might design the fourth condition by combining larger amplitude and higher frequency and evaluate their results by ANOVA; however, the carry-over effects would remain with this experimental design. It may be done as future work to see the mixed effect of amplitude and frequency.

REFERENCES

[1] M. Mori, K. MacDorman, and N. Kageki, "The Uncanny Valley [From the Field]," *IEEE Robotics & Automation Magazine*, vol. 19, pp. 98–100, June 2012.

[2] I. Pictures, "AI for Good Global Summit." `https://www.flickr.com/photos/itupictures/27254369347/`, 2018.

[3] N. Caranti, "Own work, iCub Robot." `https://commons.wikimedia.org/w/index.php?curid=69643650`, 2022.

[4] N. Abadzis, "Hugo Tate." `https://commons.wikimedia.org/wiki/File:HugoTate.jpg`, 2022.

[5] A. Rafaat, "Principles of animation." `https://edex.adobe.com/teaching-resources/vb5d12604`, June 2022.

[6] G. Hoffman, O. Zuckerman, G. Hirschberger, M. Luria, and T. S. Sherman, "Design and evaluation of a peripheral robotic conversation companion," in *Proceedings of the Tenth Annual ACM/IEEE International Conference on Human-Robot Interaction*, pp. 3–10, ACM, Mar. 2015.

[7] Y. Terzioğlu, B. Mutlu, and E. Şahin, "Designing social cues for collaborative robots: The role of gaze and breathing in human-robot collaboration," in *2020 15th ACM/IEEE International Conference on Human-Robot Interaction (HRI)*, pp. 343–357, IEEE, 2020.

[8] A. Tsoli, N. Mahmood, and M. J. Black, "Breathing life into shape: Capturing, modeling and animating 3D human breathing," *ACM Transactions on graphics (TOG)*, vol. 33, no. 4, pp. 1–11, 2014.

[9] V. B. Zordan, B. Celly, B. Chiu, and P. C. DiLorenzo, "Breathe easy: model and control of simulated respiration for animation," in *Proceedings of the 2004*

ACM SIGGRAPH/Eurographics symposium on Computer animation, pp. 29–37, 2004.

[10] S. I. Park and J. K. Hodgins, "Capturing and animating skin deformation in human motion," *ACM Transactions on Graphics (TOG)*, vol. 25, no. 3, pp. 881–889, 2006.

[11] S. Yohanan and K. E. MacLean, "A tool to study affective touch," in *CHI'09 Extended Abstracts on Human Factors in Computing Systems*, pp. 4153–4158, 2009.

[12] P. Bucci, L. Zhang, X. L. Cang, and K. E. MacLean, "Is it happy? behavioural and narrative frame complexity impact perceptions of a simple furry robot's emotions," in *Proceedings of the 2018 CHI Conference on Human Factors in Computing Systems*, pp. 1–11, 2018.

[13] P. Bucci, X. L. Cang, A. Valair, D. Marino, L. Tseng, M. Jung, J. Rantala, O. S. Schneider, and K. E. MacLean, "Sketching cuddlebits: coupled prototyping of body and behaviour for an affective robot pet," in *Proceedings of the 2017 CHI Conference on Human Factors in Computing Systems*, pp. 3681–3692, 2017.

[14] N. Yoshida and T. Yonezawa, "Investigating breathing expression of a stuffed-toy robot based on body-emotion model," in *Proceedings of the Fourth International Conference on Human Agent Interaction*, pp. 139–144, 2016.

[15] A. Asadi, O. Niebuhr, J. Jørgensen, and K. Fischer, "Inducing changes in breathing patterns using a soft robot," in *Proceedings of the 2022 ACM/IEEE International Conference on Human-Robot Interaction*, pp. 683–687, 2022.

[16] S. Yohanan and K. E. MacLean, "Design and assessment of the haptic creature's affect display," in *2011 6th ACM/IEEE International Conference on Human-Robot Interaction (HRI)*, pp. 473–480, IEEE, 2011.

[17] M. Nishi, *Breathing of Humans and its Simulation*. PhD thesis, Friedlich-Alexander-University, Cauerstr.4, D-91058 Erlangen, 6 2014.

[18] argeX, "watchx, customizable smart watch." `https://www.watchx.io/product/watchx`, 2022.

[19] IFR, "IFR presents World Robotics 2021 reports." https://ifr.org/ifr-press-releases/news/robot-sales-rise-again, 2022.

[20] International Federation of Robotics, "Demystifying collaborative industrial robots," *Frankfurt, Germany*, 2018.

[21] J. Edward, C. W. Wannasuphoprasit, and M. A. Peshkin, "Cobots: Robots for collaboration with human operators," in *International Mechanical Engineering Congress and Exposition, Atlanta*, pp. 433–440, 1996.

[22] A. Sauppé and B. Mutlu, "The social impact of a robot co-worker in industrial settings," in *Proceedings of the 33rd annual ACM conference on human factors in computing systems*, pp. 3613–3622, 2015.

[23] M. Pearce, B. Mutlu, J. Shah, and R. Radwin, "Optimizing makespan and ergonomics in integrating collaborative robots into manufacturing processes," *IEEE transactions on automation science and engineering*, vol. 15, no. 4, pp. 1772–1784, 2018.

[24] V. Villani, F. Pini, F. Leali, and C. Secchi, "Survey on human–robot collaboration in industrial settings: Safety, intuitive interfaces and applications," *Mechatronics*, vol. 55, pp. 248–266, 2018.

[25] S. Saunderson and G. Nejat, "How robots influence humans: A survey of nonverbal communication in social human–robot interaction," *International Journal of Social Robotics*, vol. 11, pp. 575–608, Jan. 2019.

[26] F. Thomas, O. Johnston, and F. Thomas, *The illusion of life: Disney animation*. Hyperion New York, 1995.

[27] T. Ribeiro and A. Paiva, "The illusion of robotic life: Principles and practices of animation for robots," in *Proceedings of the Seventh Annual ACM/IEEE International Conference on Human-Robot Interaction*, HRI '12, (New York, NY, USA), p. 383–390, Association for Computing Machinery, 2012.

[28] C. U. Press, "breathe, verb," in *Cambridge Dictionary Online*, Cambridge University Press, May 2022.

[29] S. Bloch, M. Lemeignan, and N. Aguilera-T, "Specific respiratory patterns distinguish among human basic emotions," *International Journal of Psychophysiology*, vol. 11, no. 2, pp. 141–154, 1991.

[30] V. Maric, D. Ramanathan, and J. Mishra, "Respiratory regulation & interactions with neuro-cognitive circuitry," *Neuroscience & Biobehavioral Reviews*, vol. 112, pp. 95–106, 2020.

[31] C. A. Del Negro, G. D. Funk, and J. L. Feldman, "Breathing matters," *Nature Reviews Neuroscience*, vol. 19, no. 6, pp. 351–367, 2018.

[32] Y. S. Sefidgar, K. E. MacLean, S. Yohanan, H. M. Van der Loos, E. A. Croft, and E. J. Garland, "Design and evaluation of a touch-centered calming interaction with a social robot," *IEEE Transactions on Affective Computing*, vol. 7, no. 2, pp. 108–121, 2015.

[33] A. Heloir and M. Kipp, "Real-time animation of interactive agents: Specification and realization," *Applied Artificial Intelligence*, vol. 24, no. 6, pp. 510–529, 2010.

[34] A. Shapiro, "Building a character animation system," in *International conference on motion in games*, pp. 98–109, Springer, 2011.

[35] R. C. Veltkamp and B. Piest, "A physiological torso model for realistic breathing simulation," in *3D Physiological Human Workshop*, pp. 84–94, Springer, 2009.

[36] T. A. Klausen, U. Farhadi, E. Vlachos, and J. Jørgensen, "Signalling emotions with a breathing soft robot," in *2022 IEEE 5th International Conference on Soft Robotics (RoboSoft)*, pp. 194–200, IEEE, 2022.

[37] S. Yohanan and K. E. MacLean, "The role of affective touch in human-robot interaction: Human intent and expectations in touching the haptic creature," *International Journal of Social Robotics*, vol. 4, pp. 163–180, Dec. 2011.

[38] Y. Xie and M. Matsumoto, "Emotional expression for humanoid robot using led light and breathing simulator," *IEEE Transactions on Electrical and Electronic Engineering*, 2022.

[39] H. Wu, S. Yu, and X. Yu, "3D measurement of human chest and abdomen surface based on 3d fourier transform and time phase unwrapping," *Sensors*, vol. 20, no. 4, p. 1091, 2020.

[40] A. M. Özcan, "Trust attribution in collaborative robots: An experimental investigation of non-verbal cues in a virtual human-robot interaction setting," Master's thesis, Middle East Technical University, Ankara, 6 2021.

[41] Stanford Artificial Intelligence Laboratory et al., "Robotic Operating System." `https://www.ros.org`.

[42] C. Bartneck, D. Kulić, E. Croft, and S. Zoghbi, "Measurement instruments for the anthropomorphism, animacy, likeability, perceived intelligence, and perceived safety of robots," *International Journal of Social Robotics*, vol. 1, pp. 71–81, Nov. 2008.

Appendix A

GODSPEED QUESTIONNAIRE

ANTHROPOMORPHISM

Please rate your impression of the robot on these scales

Fake	1	2	3	4	5	**Natural**
Machinelike	1	2	3	4	5	**Humanlike**
Unconscious	1	2	3	4	5	**Conscious**
Artificial	1	2	3	4	5	**Lifelike**
Moving rigidly	1	2	3	4	5	**Moving elegantly**

ANIMACY

Please rate your impression of the robot on these scales

Dead	1	2	3	4	5	**Alive**
Stagnant	1	2	3	4	5	**Lively**
Mechanical	1	2	3	4	5	**Organic**
Artificial	1	2	3	4	5	**Lifelike**
Inert	1	2	3	4	5	**Interactive**
Apathetic	1	2	3	4	5	**Responsive**

LIKEABILITY

Please rate your impression of the robot on these scales

Dislike	1	2	3	4	5	**Like**
Unfriendly	1	2	3	4	5	**Friendly**
Unkind	1	2	3	4	5	**Kind**
Unpleasant	1	2	3	4	5	**Pleasant**
Awful	1	2	3	4	5	**Nice**

PERCIEVED INTELLIGENCE

Please rate your impression of the robot on these scales

Incompetant	1	2	3	4	5	**Competent**
Ignorant	1	2	3	4	5	**Knowledgeable**
Irresponsible	1	2	3	4	5	**Responsible**
Unintelligant	1	2	3	4	5	**Intelligent**
Foolish	1	2	3	4	5	**Sensible**

PERCIEVED SAFETY

Please rate your emotional state on these scales

Anxious	1	2	3	4	5	**Relaxed**
Agitated	1	2	3	4	5	**Calm**
Quiescent	1	2	3	4	5	**Surprised**

Appendix B

DESCRIPTIVE PLOTS OF IMU DATA

Table B.1: Descriptive Statistics of Linear Accelerations at Axis 1

		Mean	Std. Deviation
mean	Amplitude Experiment	0.001	0.003
	Control (Amplitude)	0.001	0.003
	Control (Frequency)	0.002	0.002
	Frequency Experiment	0.002	0.003
standard deviation	Amplitude Experiment	0.025	0.010
	Control (Amplitude)	0.025	0.010
	Control (Frequency)	0.025	0.009
	Frequency Experiment	0.026	0.010
absolute mean	Amplitude Experiment	0.019	0.008
	Control (Amplitude)	0.019	0.008
	Control (Frequency)	0.019	0.007
	Frequency Experiment	0.019	0.008
absolute standard deviation	Amplitude Experiment	0.017	0.006
	Control (Amplitude)	0.016	0.006
	Control (Frequency)	0.016	0.006
	Frequency Experiment	0.017	0.006
absolute maximum value	Amplitude Experiment	0.099	0.033
	Control (Amplitude)	0.106	0.042
	Control (Frequency)	0.101	0.033
	Frequency Experiment	0.114	0.047
max span	Amplitude Experiment	0.178	0.060
	Control (Amplitude)	0.186	0.076
	Control (Frequency)	0.180	0.058
	Frequency Experiment	0.201	0.078

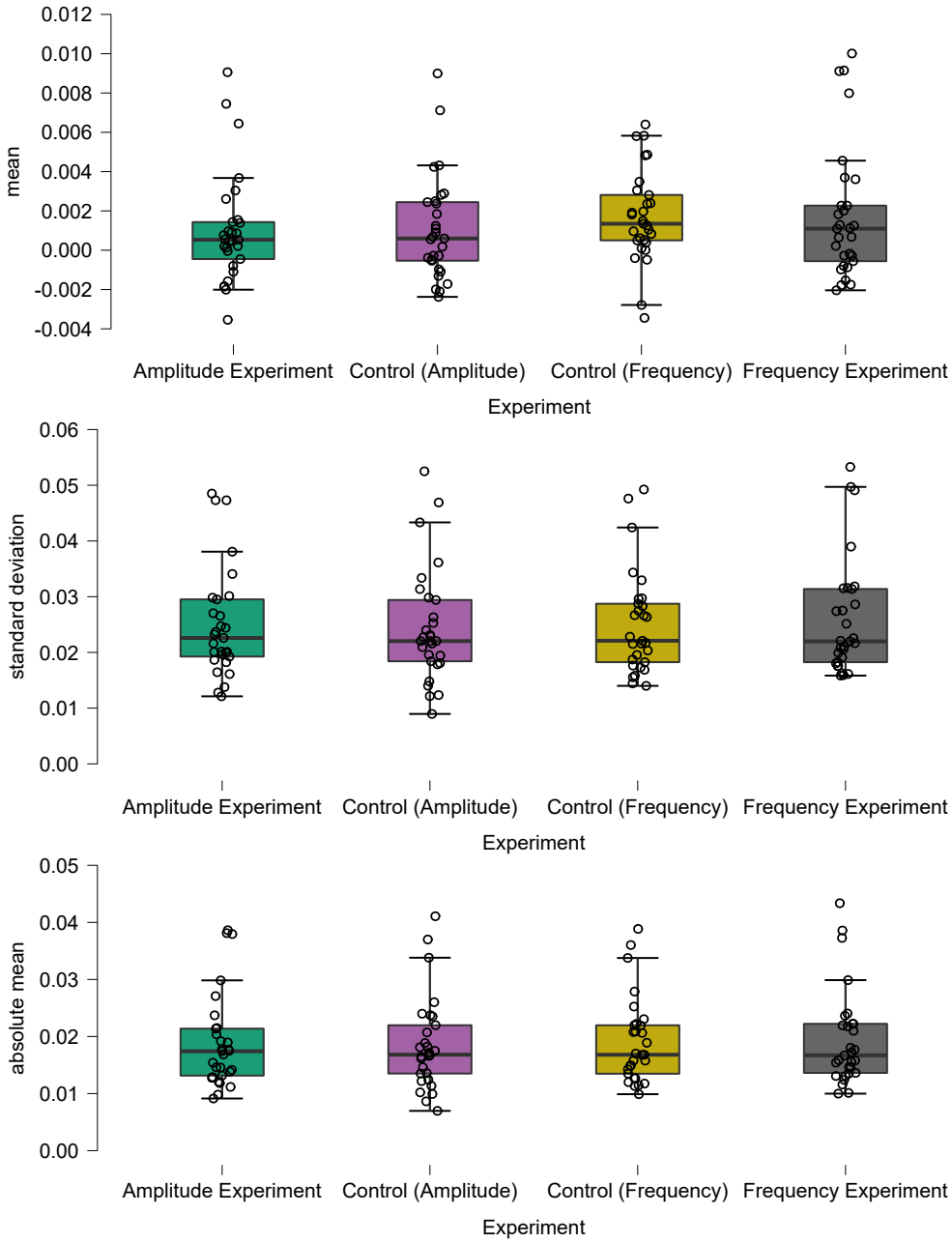

Figure B.1: Descriptive Graphics of Linear Accelerations at Axis 1 Part - 1

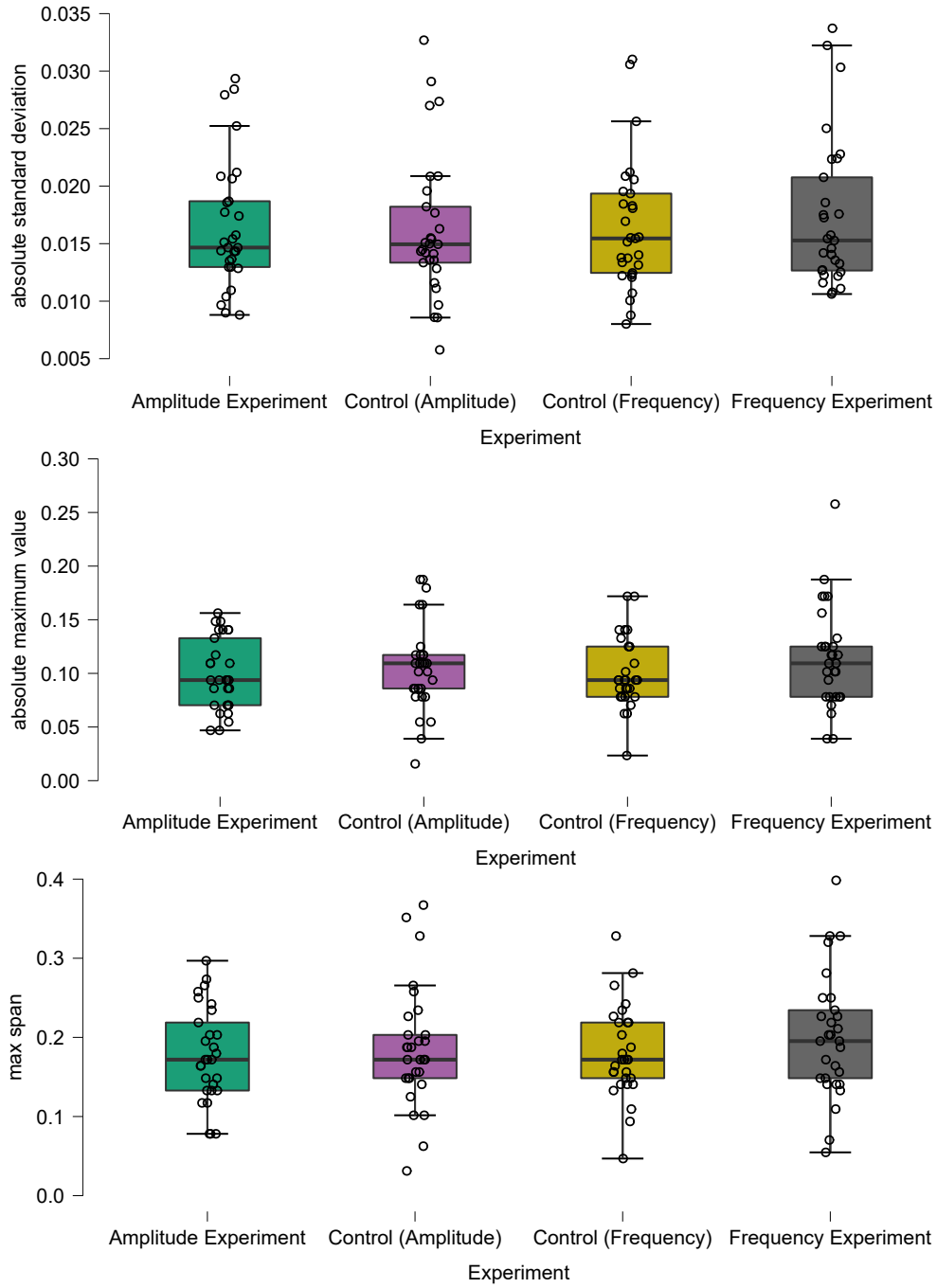

Figure B.1: Descriptive Graphics of Linear Accelerations at Axis 1 Part - 2

Table B.2: Descriptive Statistics of Linear Accelerations at Axis 2

		Mean	Std. Deviation
mean	Amplitude Experiment	−0.002	0.003
	Control (Amplitude)	−0.003	0.003
	Control (Frequency)	−0.002	0.003
	Frequency Experiment	−0.002	0.003
standard deviation	Amplitude Experiment	0.014	0.005
	Control (Amplitude)	0.014	0.005
	Control (Frequency)	0.015	0.007
	Frequency Experiment	0.014	0.006
absolute mean	Amplitude Experiment	0.010	0.005
	Control (Amplitude)	0.010	0.005
	Control (Frequency)	0.011	0.005
	Frequency Experiment	0.010	0.005
absolute standard deviation	Amplitude Experiment	0.010	0.003
	Control (Amplitude)	0.010	0.003
	Control (Frequency)	0.011	0.005
	Frequency Experiment	0.011	0.004
absolute maximum value	Amplitude Experiment	0.079	0.026
	Control (Amplitude)	0.074	0.027
	Control (Frequency)	0.079	0.040
	Frequency Experiment	0.084	0.032
max span	Amplitude Experiment	0.128	0.039
	Control (Amplitude)	0.123	0.044
	Control (Frequency)	0.128	0.059
	Frequency Experiment	0.139	0.051

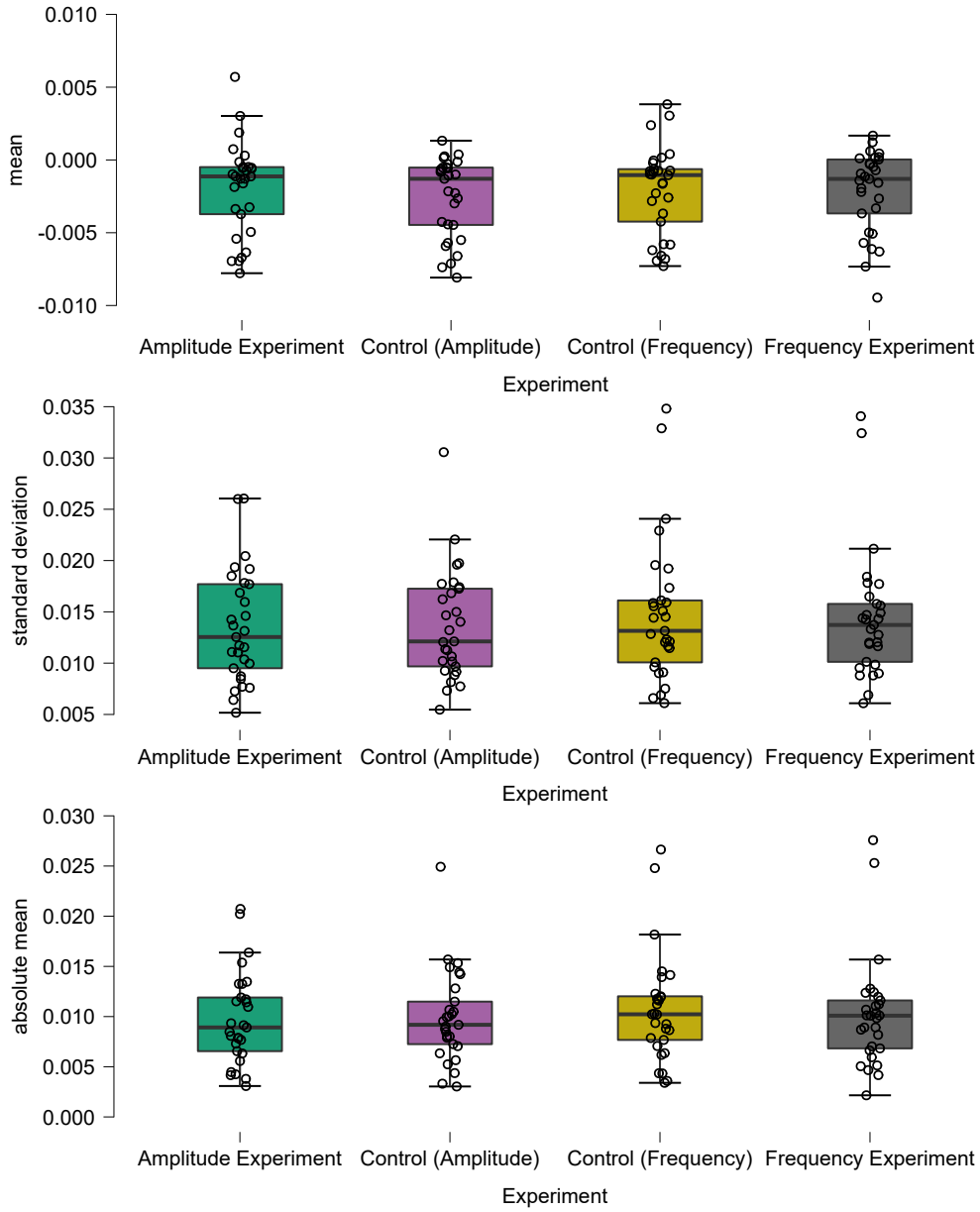

Figure B.2: Descriptive Graphics of Linear Accelerations at Axis 2 Part - 1

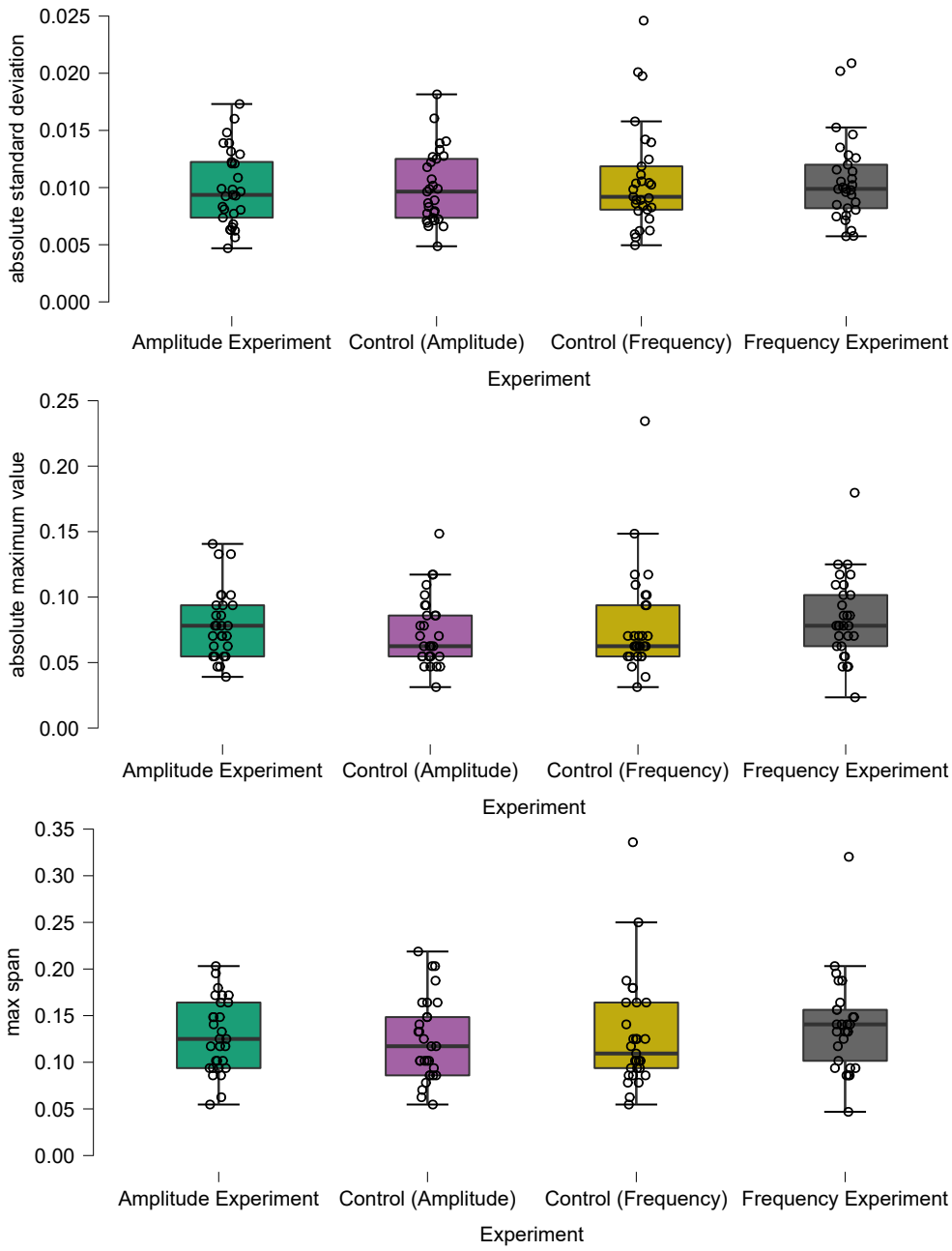

Figure B.2: Descriptive Graphics of Linear Accelerations at Axis 2 Part - 2

Table B.3: Descriptive Statistics of Linear Accelerations at Axis 3

		Mean	Std. Deviation
mean	Amplitude Experiment	0.004	0.005
	Control (Amplitude)	0.005	0.006
	Control (Frequency)	0.005	0.005
	Frequency Experiment	0.004	0.005
standard deviation	Amplitude Experiment	0.023	0.011
	Control (Amplitude)	0.024	0.009
	Control (Frequency)	0.022	0.007
	Frequency Experiment	0.024	0.010
absolute mean	Amplitude Experiment	0.018	0.006
	Control (Amplitude)	0.018	0.006
	Control (Frequency)	0.018	0.006
	Frequency Experiment	0.018	0.006
absolute standard deviation	Amplitude Experiment	0.016	0.010
	Control (Amplitude)	0.016	0.007
	Control (Frequency)	0.015	0.004
	Frequency Experiment	0.017	0.008
absolute maximum value	Amplitude Experiment	0.119	0.141
	Control (Amplitude)	0.120	0.139
	Control (Frequency)	0.092	0.039
	Frequency Experiment	0.151	0.195
max span	Amplitude Experiment	0.189	0.149
	Control (Amplitude)	0.191	0.145
	Control (Frequency)	0.159	0.059
	Frequency Experiment	0.221	0.197

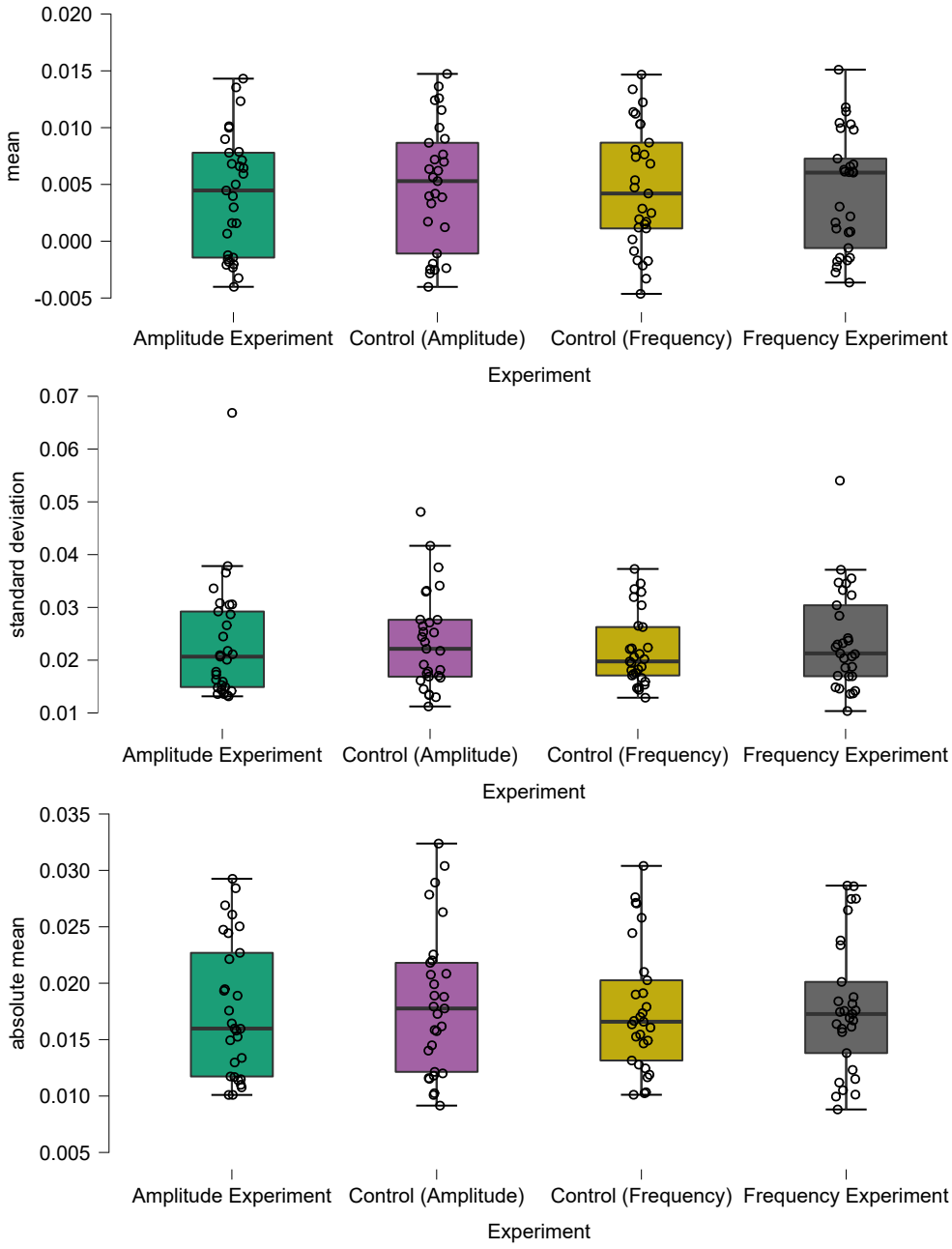

Figure B.3: Descriptive Graphics of Linear Accelerations at Axis 3 Part - 1

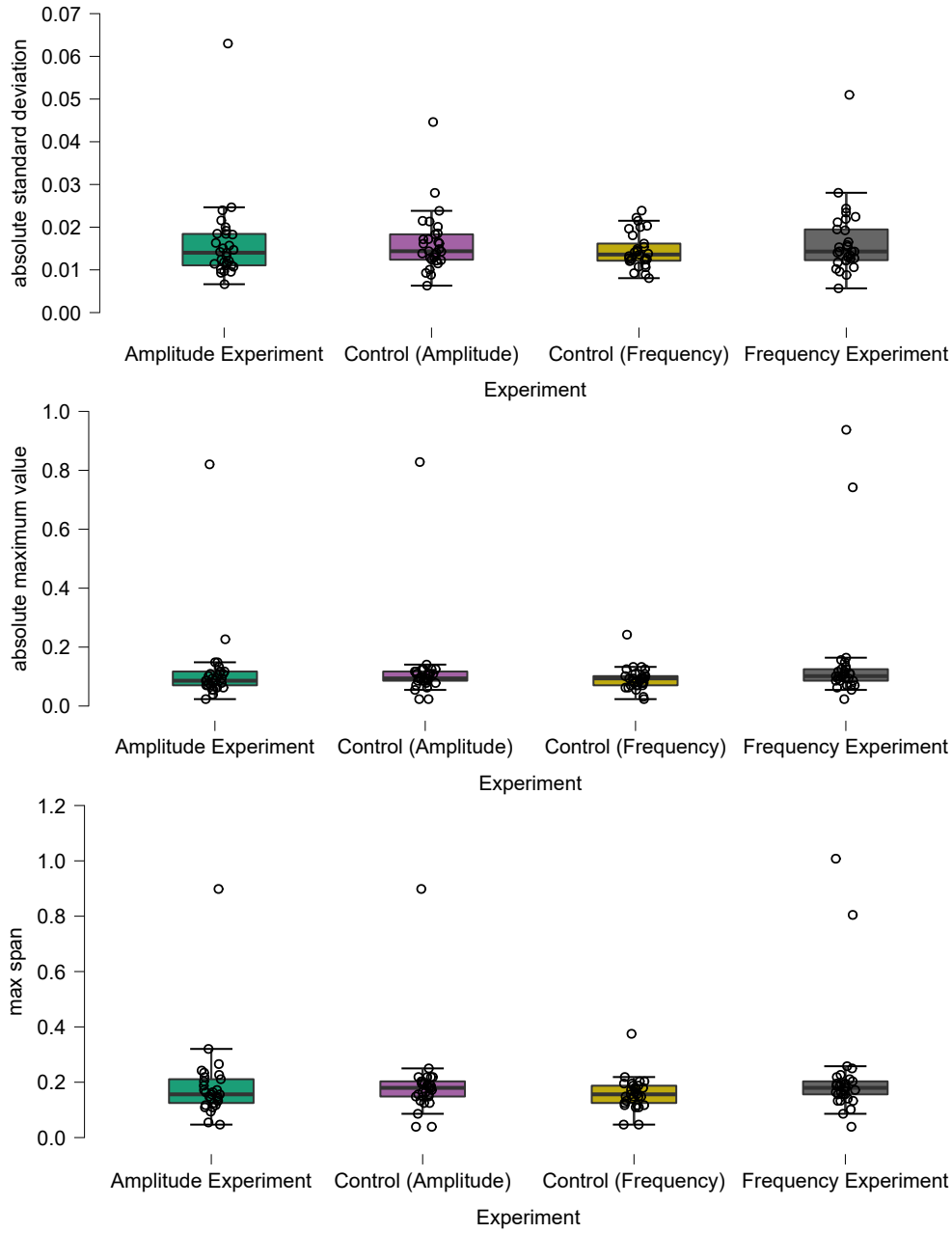

Figure B.3: Descriptive Graphics of Linear Accelerations at Axis 3 Part - 2

Table B.4: Descriptive Statistics of Angular Velocities at Axis 1

		Mean	Std. Deviation
mean	Amplitude Experiment	-0.004	0.050
	Control (Amplitude)	-0.013	0.040
	Control (Frequency)	-0.002	0.059
	Frequency Experiment	$-8.568e-4$	0.051
standard deviation	Amplitude Experiment	10.867	6.637
	Control (Amplitude)	12.345	5.945
	Control (Frequency)	10.849	7.931
	Frequency Experiment	9.921	6.534
absolute mean	Amplitude Experiment	3.749	3.276
	Control (Amplitude)	4.268	2.939
	Control (Frequency)	4.044	3.784
	Frequency Experiment	3.320	2.890
absolute standard deviation	Amplitude Experiment	10.126	5.880
	Control (Amplitude)	11.519	5.283
	Control (Frequency)	9.991	7.058
	Frequency Experiment	9.298	5.922
absolute maximum value	Amplitude Experiment	51.634	13.526
	Control (Amplitude)	53.498	10.120
	Control (Frequency)	47.625	19.080
	Frequency Experiment	49.631	15.664
max span	Amplitude Experiment	101.226	27.746
	Control (Amplitude)	105.802	20.517
	Control (Frequency)	93.767	37.795
	Frequency Experiment	97.279	31.921

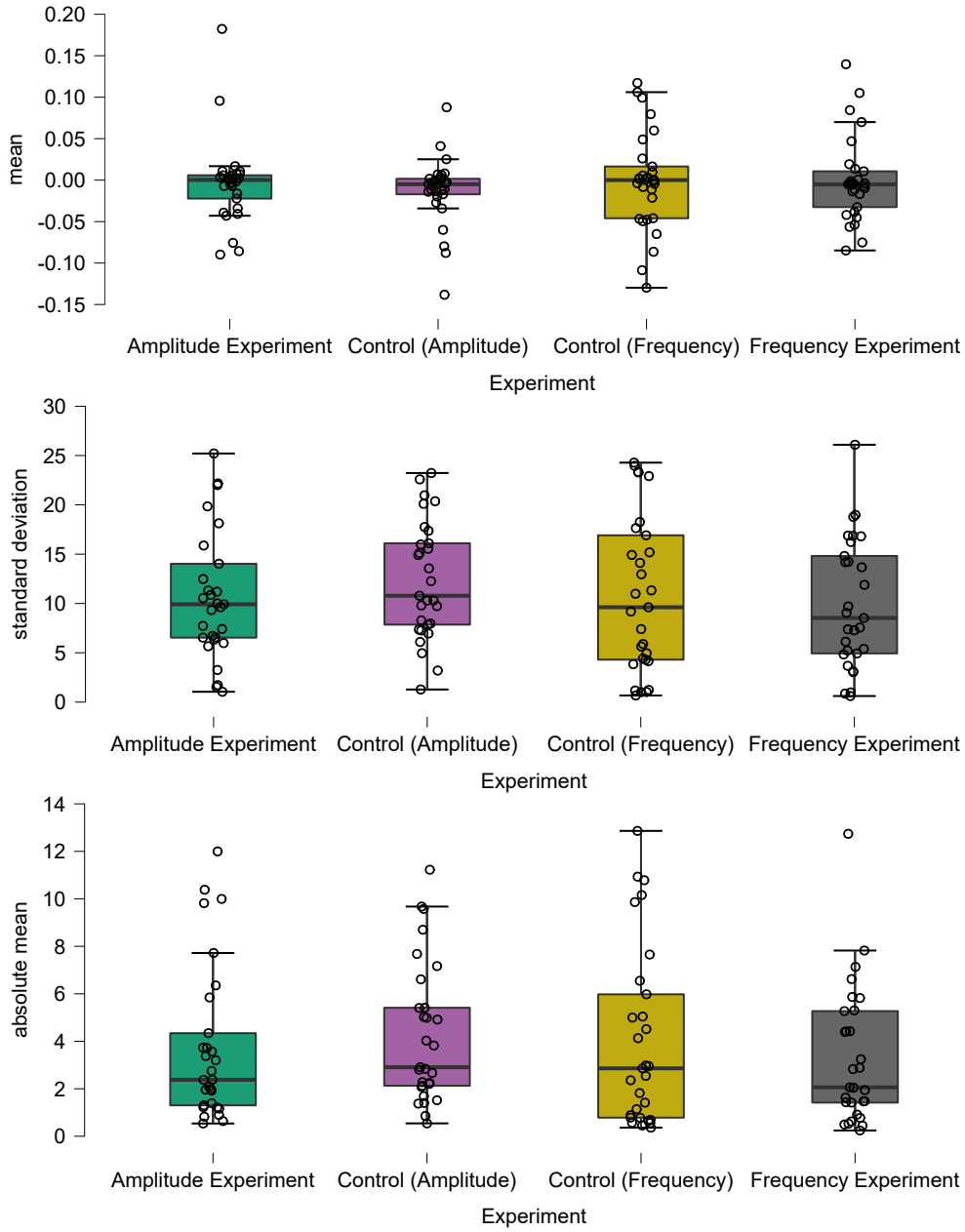

Figure B.4: Descriptive Graphics of Angular Velocities at Axis 1 Part - 1

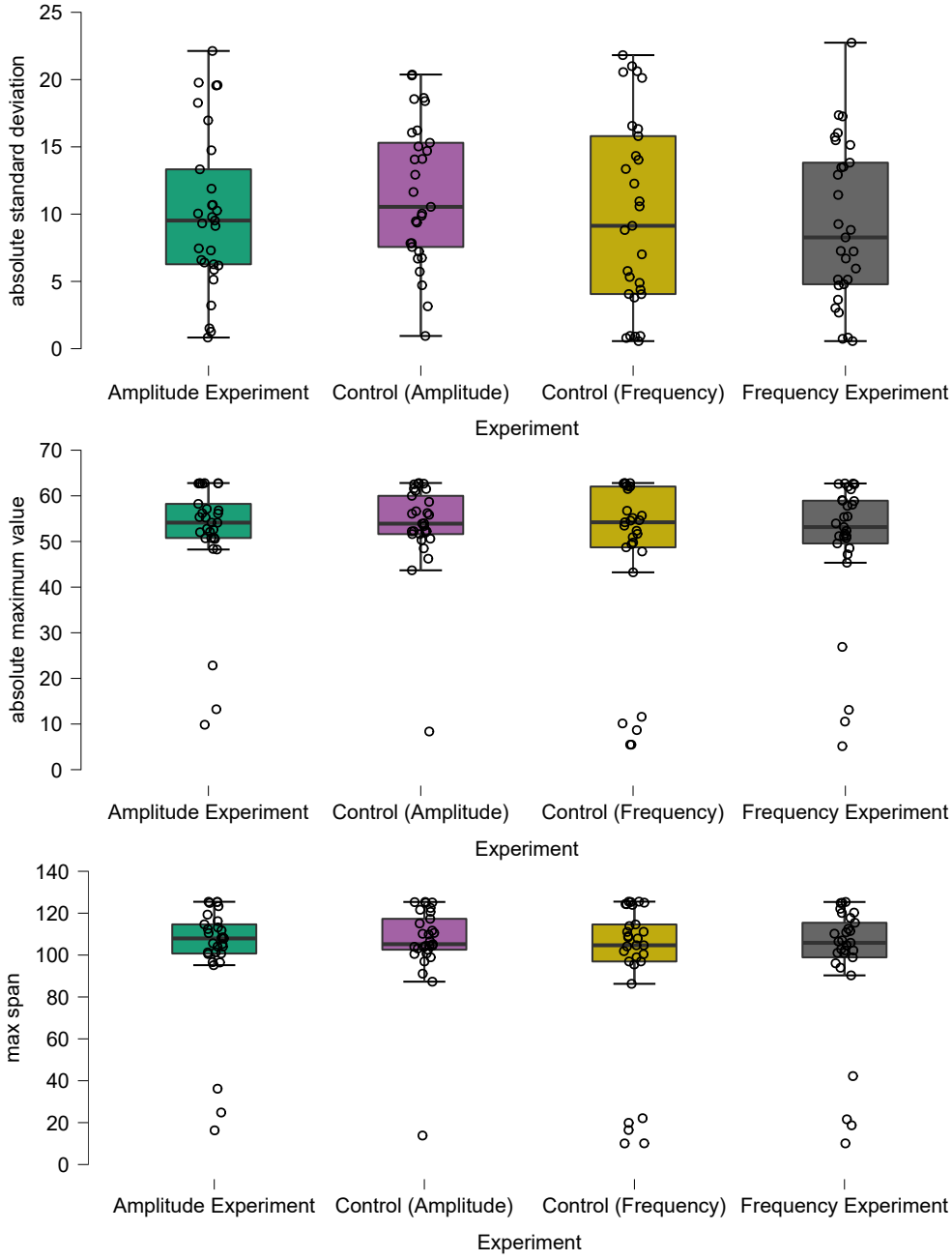

Figure B.4: Descriptive Graphics of Angular Velocities at Axis 1 Part - 2

Table B.5: Descriptive Statistics of Angular Velocities at Axis 2

		Mean	Std. Deviation
mean	Amplitude Experiment	−0.004	0.026
	Control (Amplitude)	0.003	0.027
	Control (Frequency)	−0.005	0.026
	Frequency Experiment	−0.004	0.022
standard deviation	Amplitude Experiment	5.737	3.443
	Control (Amplitude)	5.416	3.668
	Control (Frequency)	5.517	3.235
	Frequency Experiment	5.647	3.508
absolute mean	Amplitude Experiment	2.363	1.709
	Control (Amplitude)	2.295	1.981
	Control (Frequency)	2.202	1.568
	Frequency Experiment	2.327	1.656
absolute standard deviation	Amplitude Experiment	5.180	3.061
	Control (Amplitude)	4.853	3.160
	Control (Frequency)	5.021	2.885
	Frequency Experiment	5.110	3.139
absolute maximum value	Amplitude Experiment	25.850	7.308
	Control (Amplitude)	26.065	7.104
	Control (Frequency)	25.515	7.814
	Frequency Experiment	26.371	6.973
max span	Amplitude Experiment	50.226	14.575
	Control (Amplitude)	49.872	14.385
	Control (Frequency)	49.765	15.797
	Frequency Experiment	50.839	14.954

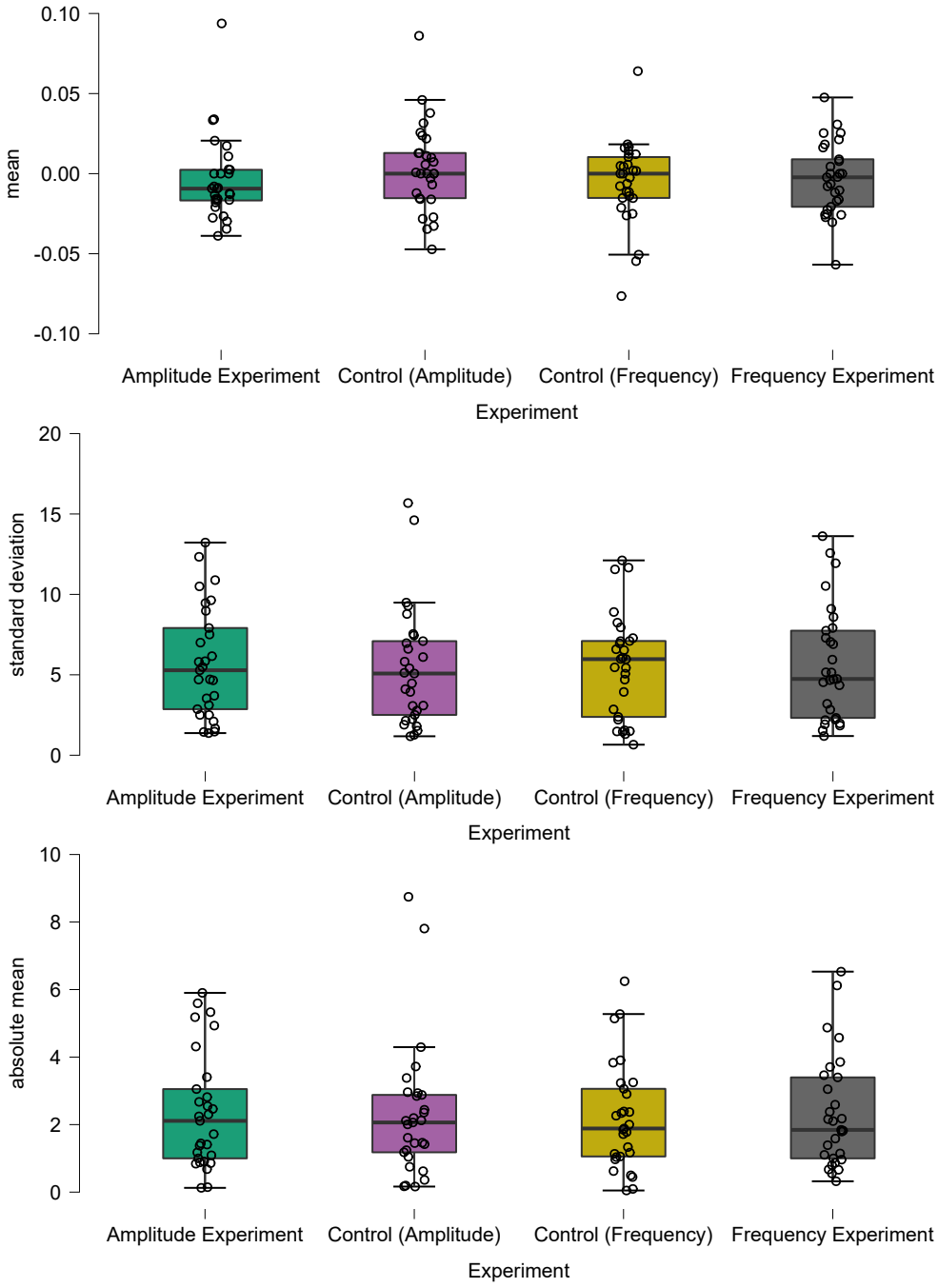

Figure B.5: Descriptive Graphics of Angular Velocities at Axis 2 Part - 1

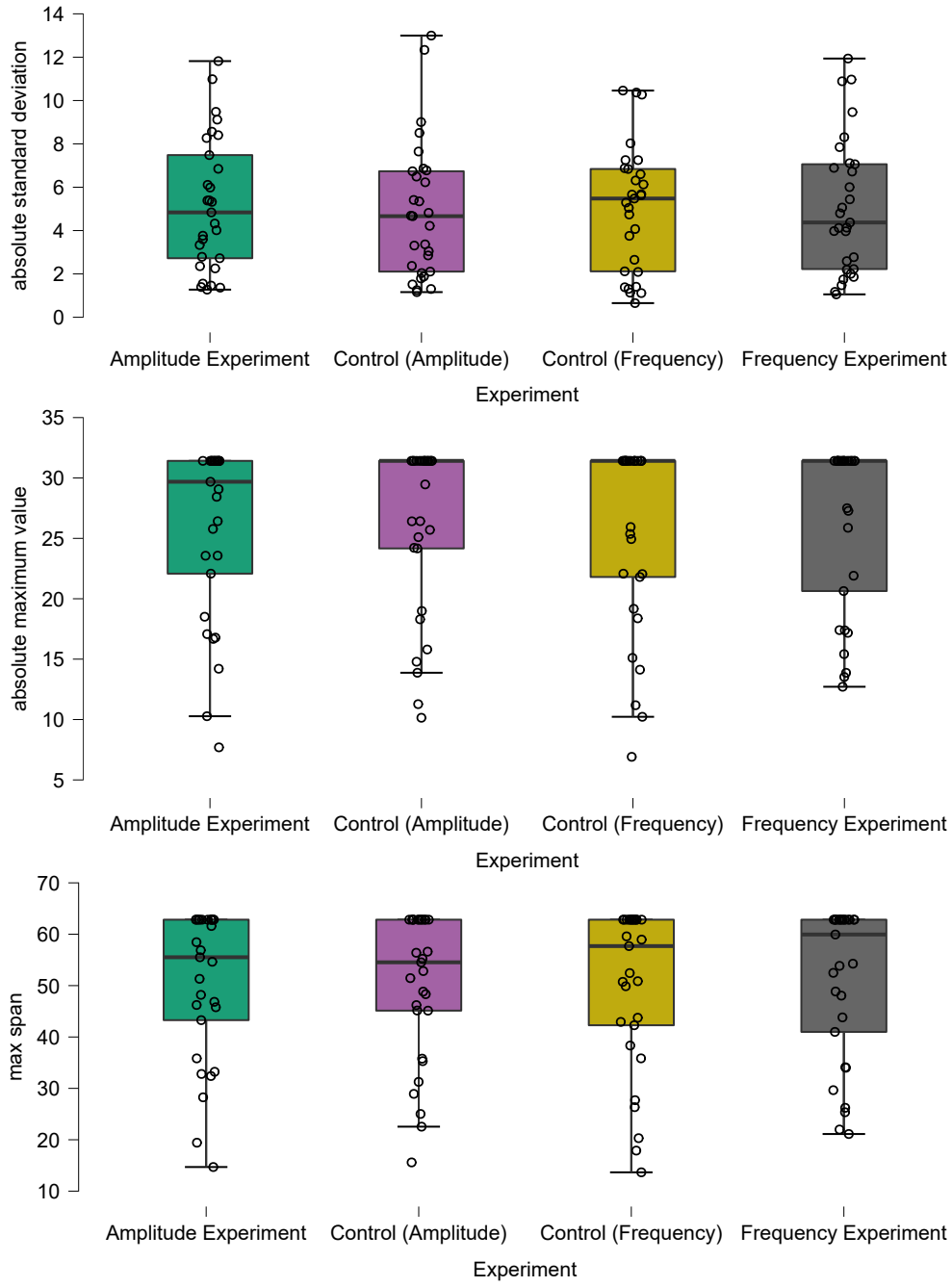

Figure B.5: Descriptive Graphics of Angular Velocities at Axis 2 Part - 2

Table B.6: Descriptive Statistics of Angular Velocities at Axis 3

		Mean	Std. Deviation
mean	Amplitude Experiment	0.007	0.031
	Control (Amplitude)	−0.008	0.051
	Control (Frequency)	−0.002	0.075
	Frequency Experiment	0.006	0.061
standard deviation	Amplitude Experiment 12.441	6.013	
	Control (Amplitude)	11.872	6.394
	Control (Frequency)	12.102	7.406
	Frequency Experiment	11.011	6.629
absolute mean	Amplitude Experiment 4.550	3.182	
	Control (Amplitude)	4.206	3.149
	Control (Frequency)	4.580	3.811
	Frequency Experiment	3.916	3.012
absolute standard deviation	Amplitude Experiment	11.482	5.296
	Control (Amplitude)	11.026	5.696
	Control (Frequency)	11.104	6.498
	Frequency Experiment	10.223	6.002
absolute maximum value	Amplitude Experiment	54.733	12.062
	Control (Amplitude)	52.905	12.382
	Control (Frequency)	50.952	14.340
	Frequency Experiment	50.892	13.594
max span	Amplitude Experiment	107.212	24.552
	Control (Amplitude)	103.457	25.143
	Control (Frequency)	100.356	28.681
	Frequency Experiment	98.327	29.615

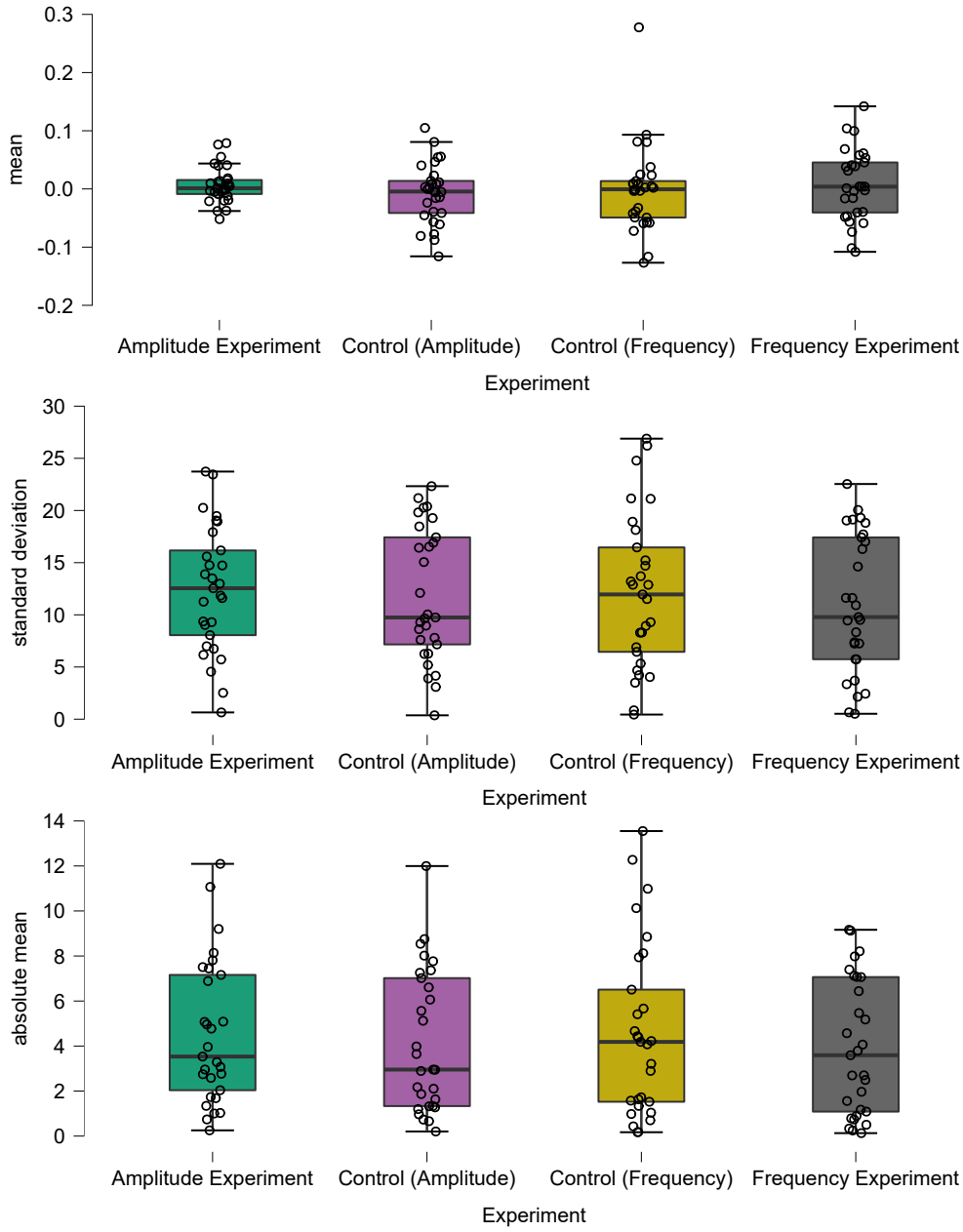

Figure B.6: Descriptive Graphics of Angular Velocities at Axis 3 Part - 1

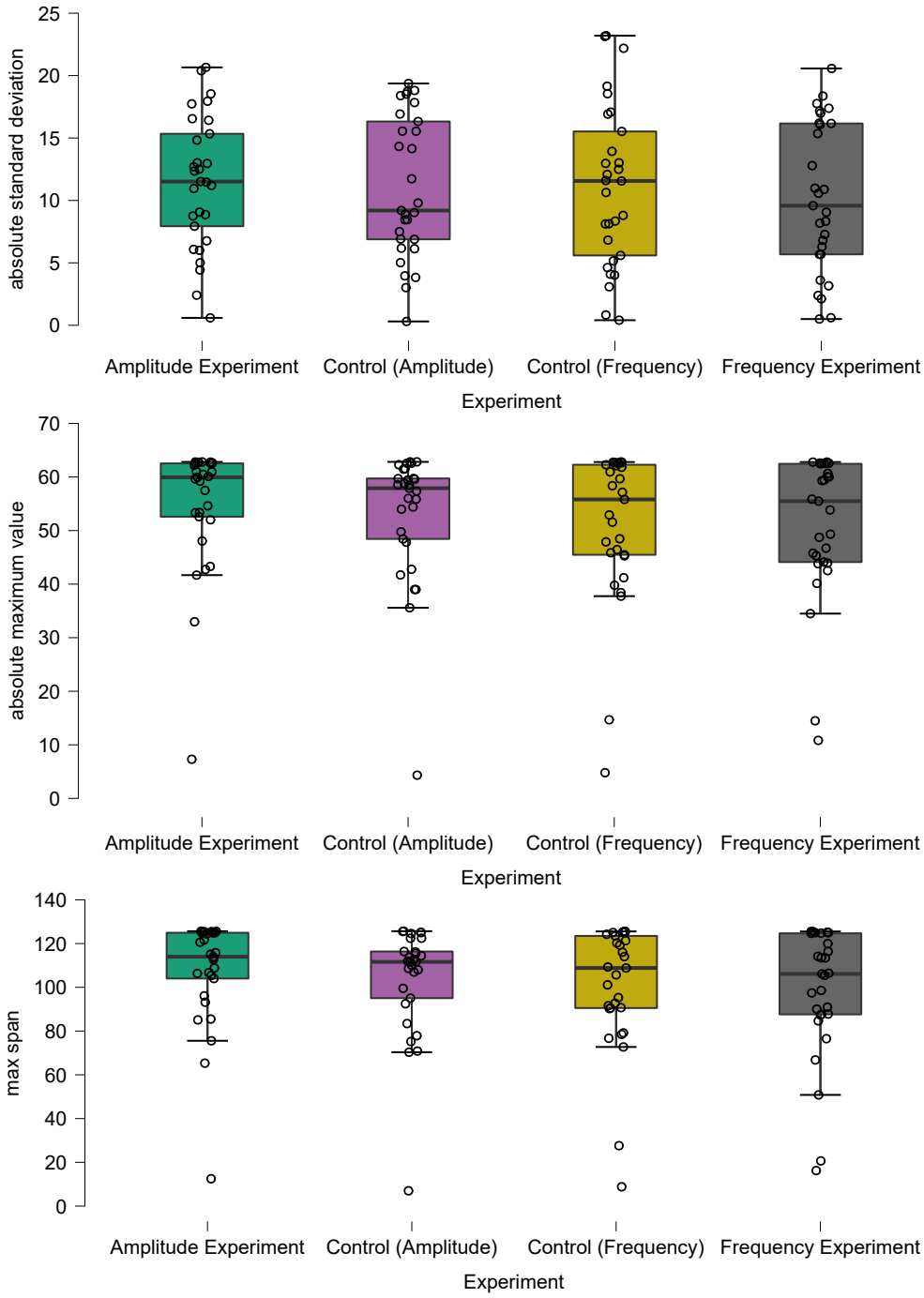

Figure B.6: Descriptive Graphics of Angular Velocities at Axis 3 Part - 2